ION–SOLID INTERACTIONS: FUNDAMENTALS AND APPLICATIONS

CAMBRIDGE SOLID STATE SCIENCE SERIES

EDITORS

Professor D. R. Clarke
Department of Materials Science and Engineering,
University of California, Santa Barbara

Professor S. Suresh
Department of Materials Science and Engineering,
Massachusetts Institute of Technology

Professor I. M. Ward FRS
IRC in Polymer Science and Technology,
University of Leeds

and the Lindhard formulation

$$a_L = \frac{0.8853a_0}{(Z_1^{2/3} + Z_2^{2/3})^{1/2}}$$

Compare these values with the 'universal' value

$$a_U = \frac{0.8854a_0}{(Z_1^{0.23} + Z_2^{0.23})}$$

2.2 Calculate the value of the screening function $\chi(r/a)$ at values of $x = r/a = 1$, 5, 10, and 15 for the Sommerfeld (Eq. (2.30)), the Moliere (Eq. (2.36)) and the Lenz–Jensen (Eq. (2.39)) forms.

2.3 Plot the Lennard–Jones potential from $r = 0.8a_0$ to $r = 4a_0$ for Cu with $\varepsilon_b = 0.6$ eV/atom, where a_0 = Bohr radius.

2.4 From values of the binding energy E_b for 1 mol. obtained from the cohesive energy, calculate the minimum potential energy ε_b for Al (fcc), $E_b = 3.39$ eV/atom; Si (diam. cubic), $E_b = 4.63$ eV/atom; and for W(bcc), $E_b = 8.90$ eV/atom.

2.5 Using values of the thermal expansion coefficient, Young's modulus, and melting temperature, compare the relative shapes of the interatomic potentials for Cu, W, and Si.

3

Dynamics of binary elastic collisions

3.1 Introduction

In ion beam modification of materials, the energetic ions interact with the solid through forces which can be described by the ion–target atom interatomic potential. These interactions are the basis of development of expressions for ion range and ion damage in solids. Consider the passage of an energetic ion in a solid during an ion implantation experiment, Fig. 3.1. As the ion transverses the solid it undergoes collisions with the stationary target atoms, which deflect the ion from its initial direction. The ion also collides with electrons in the solid and loses energy in these collisions. The major changes in its flight

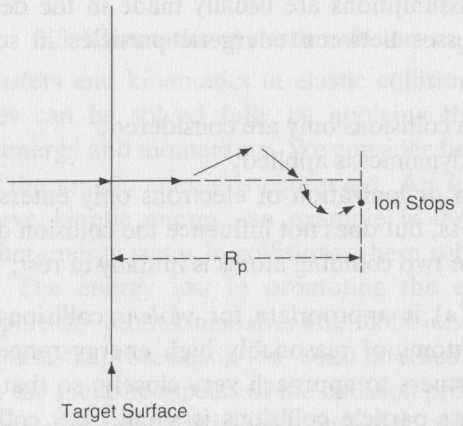

Fig. 3.1. The passage of an energetic ion in a solid during an ion implantation experiment, showing the total ion path and the projected range, R_p. As the ion transverses the solid, it undergoes collisions with the stationary target atoms, which deflect the ion from its initial direction.

direction are due to the ion's collision with individual lattice atoms. In this chapter we will focus on two-body collisions or binary collisions involving energetic ions and target atoms.

The simplest collision event is the collision between a charged particle and the atomic nucleus. This can be treated as a two-body collision provided that the mean free path between collisions is much greater than the interatomic spacing. The chance of correlation effects due to neighboring atoms recoiling simultaneously is then very small. The momentum of the recoiling target atoms is the parameter which determines the amount of damage that occurs in the solid target. The momentum transferred to the recoiling atom is also responsible for a large portion of the energy-loss process of the ion.

In developing our understanding of ion–solid interactions for the purposes of ion beam modification of materials, we will first derive some general relations governing two-body collisions, considering only the asymptotic values of momentum at great distances from the collision. The principles of conservation of momentum and energy are all that are required to obtain recoil energy as a function of recoil angle. We shall assume that collisions are elastic and, further, that velocities are small enough for non-relativistic mechanics to apply.

3.2 Classical scattering theory

The following assumptions are usually made in the description of the scattering processes between energetic particles in solids (Sigmund, 1972):

(a) two-atom collisions only are considered;
(b) classical dynamics is applied;
(c) excitation or ionization of electrons only enters as a source of energy loss, but does not influence the collision dynamics;
(d) one of the two colliding atoms is initially at rest;

Assumption (a) is appropriate for *violent* collisions. Violent collisions between atoms of reasonably high energy range (keV) require the collision partners to approach very closely, so that the probability for three-or-more-particle collisions is small. *Soft* collisions can take place at large distances, and therefore can involve more than two atoms simultaneously. However, soft collisions can usually be treated by perturbation theory (the momentum or impulse approximation, see

Section 4.4), in which case no restriction to binary collisions is necessary. At lower energies (below 1 keV), collective effects become increasingly important and assumption (a) starts to break down. However, the problems associated with many-body collisions in this low-energy regime can be overcome by molecular-dynamic simulations where assumption (a) is not required.

In the limit of assumption (b), the applicability of classical mechanics is normally limited to specific quantities, one of which is the differential scattering cross-section $d\sigma(\theta_c)$, where θ_c is the center-of-mass scattering angle.

Neglecting the effect of electronic excitation on the collision dynamics, assumption (c) is justified if either the energy transferred to electrons is small compared with the exchange of kinetic energy between the atoms (so that the scattering angle can be calculated by assuming elastic collisions), or if no appreciable deflection takes place. In either case, the electronic energy loss enters as a superimposed energy absorption.

The assumption of one collision partner being at rest initially, assumption (d), has been made in all previous work except molecular-dynamics computations. It is not fulfilled in very dense collision cascades, especially when the process of energy dissipation has proceeded to the point where most of the atoms in the cascade are in motion.

3.3 Kinematics of elastic collisions

The energy transfers and kinematics in elastic collisions between two isolated particles can be solved fully by applying the principles of conservation of energy and momentum. We consider those collisions as *elastic* in which the kinetic energy is conserved. An *inelastic* collision does not conserve kinetic energy; an example is the promotion of electrons to higher-energy states in collisions where substantial K-shell overlap occurs. The energy lost in promoting the electrons is not available in the particle–atom kinematics after collision. In this chapter we consider only elastic processes in ion–solid interactions. In Chapter 5 we will discuss the inelastic aspects of the collision process.

For an incident energetic particle of mass M_1, the values of the velocity and energy are v_0 and E_0 ($E_0 = (1/2)M_1v_0^2$), while the target atoms of mass M_2 are at rest. After the collision, the values of the velocities v_1 and v_2 and energies E_1 and E_2 of the projectile and target

atoms, respectively, are determined by the scattering angle θ and recoil angle ϕ. The notation and geometry for the laboratory system of coordinates are given in Fig. 3.2. Table 3.1 lists those symbols used in kinematic expressions.

Conservation of energy and conservation of momentum parallel and perpendicular to the direction of incidence are expressed by the equations

$$E_0 = \tfrac{1}{2}M_1v_0^2 = \tfrac{1}{2}M_1v_1^2 + \tfrac{1}{2}M_2v_2^2 \tag{3.1}$$

$$M_1v_0 = M_1v_1\cos\theta + M_2v_2\cos\phi \tag{3.2}$$

$$0 = M_1v_1\sin\theta - M_2v_2\sin\phi \tag{3.3}$$

These three equations, (3.1)–(3.3), can be solved in various forms. For example, transposing the first term on the right to the left side in Eqs. (3.2) and (3.3), squaring and adding, will eliminate ϕ, giving

$$(M_2v_2)^2 = (M_1v_0)^2 + (M_1v_1)^2 - 2M_1^2v_0v_1\cos\theta \tag{3.4}$$

Substituting Eq. (3.4) into Eq. (3.1) to eliminate v_2, one finds the ratio of the particle's velocity before the collision to that after the collision:

$$\frac{v_1}{v_0} = \frac{M_1}{M_1 + M_2}\cos\theta \pm \left[\left(\frac{M_1}{M_1 + M_2}\right)^2\cos^2\theta + \frac{M_2 - M_1}{M_1 + M_2}\right]^{1/2} \tag{3.5}$$

Eq. (3.5) can be used with Eq. (3.4) to determine v_2 and E_2, and it can be used with Eq. (3.2) to find the angle of recoil, ϕ, of the scattered target atom.

If $M_1 > M_2$, the quantity under the radical in Eq. (3.5) will be zero for $\theta = \theta_m$, where θ_m is found from:

$$\cos^2\theta_m = 1 - \frac{M_2^2}{M_1^2}, \quad 0 \leqslant \theta_m \leqslant \frac{\pi}{2} \tag{3.6}$$

For $\theta > \theta_m$ (and $\theta \leqslant \pi$), v_1/v_0 is either imaginary or negative, neither of which is physical, so that θ_m represents the maximum angle through which M_1 can be scattered.

For the condition $M_1 < M_2$, all values of θ from 0 to π are possible, and a positive value for v_1/v_0 results if the plus sign in Eq. (3.5) is chosen. Choice of the minus sign in this equation leads to negative values of v_1/v_0, which is physically unrealistic. The ratio of the projectile energies for $M_1 < M_2$, where the plus sign holds, is

$$\frac{E_1}{E_0} = \left[\frac{(M_2^2 - M_1^2\sin^2\theta)^{1/2} + M_1\cos\theta}{M_2 + M_1}\right]^2 \tag{3.7}$$

Additional relationships between energy and scattering angles are given in Table 3.2.

Table 3.1. *Definitions and symbols used in collision kinematics*

E_0	energy of the incident projectile
E_c	total kinetic energy in the center-of-mass system
E_1	laboratory energy of the scattered projectile
E_2	laboratory energy of the recoiling target
T	energy E_2 transferred to the target atom
θ_c	center-of-mass variable scattering angle defined in Fig. 3.7
K	backscattering kinematic factor E_1/E_0
M_1	mass of the incident projectile
M_2	mass of the target particle
M_c	reduced mass in center-of-mass system
μ	mass ratio M_1/M_2
v_0	velocity of the incident projectile in laboratory coordinates
v_1	velocity of the scattered projectile in laboratory coordinates
v_2	velocity of the recoiling atom in laboratory coordinates
v_c	velocity of the reduced mass in center-of-mass coordinates
v_{ion}	velocity of the incident projectile (ion) in center-of-mass coordinates
v_{atom}	velocity of the target atom in center-of-mass coordinates
θ	laboratory angle of the scattered projectile
θ_c	center-of-mass angle of the scattered projectile
θ_m	maximum laboratory angle for M_1 scattering ($M_1 > M_2$)
ϕ	laboratory angle of the recoiling target atom
ϕ_c	center-of-mass angle of the recoiling target atom
π	$\pi = 180° = \theta_c + \phi_c$

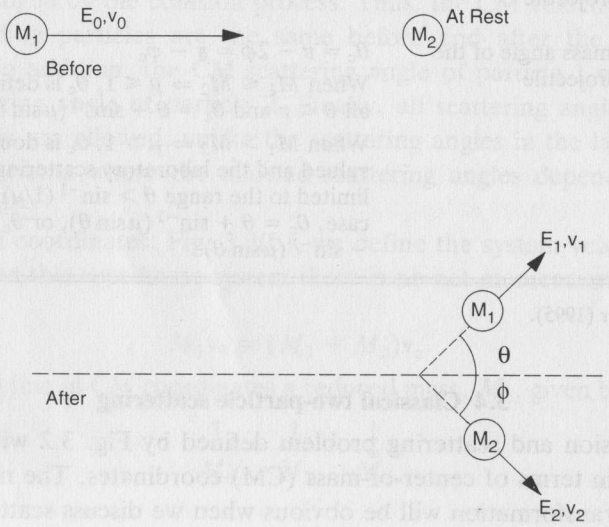

Fig. 3.2. Elastic collision diagram between two unequal masses as seen in the laboratory reference frame.

Table 3.2. *Relationships between energy and scattering angles*

Centre-of-mass energy	$E_c = \dfrac{M_2 E_0}{M_1 + M_2} = \dfrac{E_0}{1+\mu,}; \mu = \dfrac{M_1}{M_2}$
Laboratory energy of the scattered projectile for $M_1 \leqslant M_2$	$K = \dfrac{E_1}{E_0} = \dfrac{[\mu\cos\theta + (1-\mu^2\sin^2\theta)^{1/2}]^2}{(1+\mu)^2}$ When $M_1 = M_2$, $\theta \leqslant \dfrac{\pi}{2}$
Laboratory energies of the scattered projectile for $M_1 > M_2$	$\dfrac{E_1}{E_0} = \dfrac{[\mu\cos\theta \pm (1-\mu^2\sin^2\theta)^{1/2}]^2}{(1+\mu)^2}$ $\theta \leqslant \sin^{-1}(1/\mu)$
Laboratory energy of the recoil nucleus	$\dfrac{E_2}{E_0} = 1 - \dfrac{E_1}{E_0} = \dfrac{4M_1M_2}{(M_1+M_2)^2}\cos^2\phi$ $= \dfrac{4\mu}{(1+\mu)^2}\cos^2\phi = \dfrac{4\mu}{(1+\mu)^2}\sin^2\left(\dfrac{\theta_c}{2}\right)$ where $\phi \leqslant \dfrac{\pi}{2}$
Laboratory angle of the recoil nucleus	$\phi = \dfrac{\pi - \theta_c}{2} = \dfrac{\phi_c}{2}; \quad \sin\phi = \left(\dfrac{M_1E_1}{M_2E_2}\right)^{1/2}\sin\theta$
Laboratory angle of the scattered projectile	$\tan\theta = \dfrac{M_2\sin\theta_c}{M_1 + M_2\cos\theta_c}$
Center-of-mass angle of the scattered projectile	$\theta_c = \pi - 2\phi = \pi - \phi_c$ When $M_1 \leqslant M_2 \Rightarrow \mu \leqslant 1$, θ_c is defined for all $\theta \leqslant \pi$ and $\theta_c = \theta + \sin^{-1}(\mu\sin\theta)$ When $M_1 > M_2 \Rightarrow \mu > 1$, θ_c is double valued and the laboratory scattering angle is limited to the range $\theta > \sin^{-1}(1/\mu)$. In this case, $\theta_c = \theta + \sin^{-1}(\mu\sin\theta)$, or $\theta_c = \pi + \theta - \sin^{-1}(\mu\sin\theta)$

After Weller (1995).

3.4 Classical two-particle scattering

The collision and scattering problem defined by Fig. 3.2 will now be restated in terms of center-of-mass (CM) coordinates. The motivation for this transformation will be obvious when we discuss scattering in a central force field later in this chapter. Through the use of CM coordinates it will be shown that no matter how complex the force is

between the two particles, so long as it acts only along the line joining them (no transverse forces), the relative motion of the two particles can be reduced to that of a single particle moving in an interatomic potential centered at the origin of the center-of-mass coordinates. By introducing the CM system, the mutual interaction of the two colliding particles can be described by a force field, $V(r)$, which depends only on the absolute value of the interatomic separation, r. The motion of both particles is given by one equation of motion. This equation has r as the independent variable and describes a particle moving in the central force field $V(r)$.

The CM coordinates for a two-particle system are defined in a zero-momentum reference frame. In the frame, the total force on two particles that interact only with each other is zero. Since we can define the total force of two interacting particles as

$$\mathbf{F_T} = \mathbf{F_1} + \mathbf{F_2} = \frac{d\mathbf{p_T}}{dt} \tag{3.8}$$

where $\mathbf{F_T}$ = total force, $\mathbf{F_1}$ and $\mathbf{F_2}$ are the individual forces on particles 1 and 2, respectively, and $\mathbf{p_T}$ is the total linear momentum of the two-particle system. For $\mathbf{F_T} = 0$, $d\mathbf{p_T} = 0$, indicating that the total momentum is unchanged or conserved during the interaction process.

One of the consequences associated with observing elastic collisions in the CM coordinates is that the individual particle kinetic energies are unchanged by the collision process. Thus, the CM velocities of the two colliding particles are the same before and after the collision process. In addition, the CM scattering angle of particle 1 will equal the scattering angle of particle 2. Finally, all scattering angles in the CM system are allowed, unlike the scattering angles in the laboratory reference frame where the allowed scattering angles depend on the ratio M_1/M_2.

For CM coordinates, Fig. 3.3(b), we define the system velocity, v_c, such that in this coordinate system there is no net momentum change, so that

$$M_1\mathbf{v_0} = (M_1 + M_2)\mathbf{v_c} \tag{3.9}$$

We also define in CM coordinates a reduced mass, M_c, given by

$$\frac{1}{M_c} = \frac{1}{M_1} + \frac{1}{M_2} \tag{3.10}$$

or

$$M_c = \frac{M_1M_2}{M_1 + M_2} \tag{3.11}$$

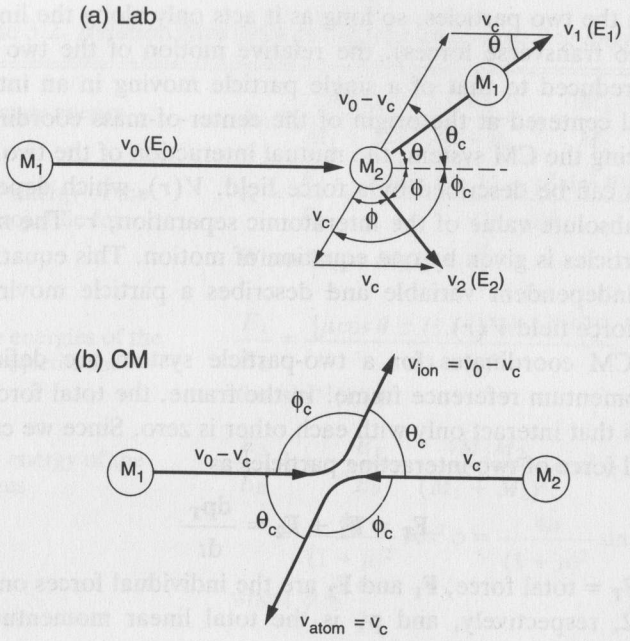

Fig. 3.3. Elastic collision diagrams between two unequal masses as seen in the (a) laboratory reference frame and (b) CM reference frame.

From Eqs. (3.9) and (3.11) we can represent the CM velocity in terms of reduced mass as

$$\mathbf{v_c} = \mathbf{v_0}\frac{M_c}{M_2} \tag{3.12}$$

From the velocity vector diagram in Fig. 3.3 and Eq. (3.12), the ion and target atom velocities in CM coordinates are

$$\mathbf{v_{ion}} = \mathbf{v_0} - \mathbf{v_c} = \mathbf{v_0}\frac{M_c}{M_1} \tag{3.13}$$

$$\mathbf{v_{atom}} = \mathbf{v_c} = \mathbf{v_0}\frac{M_c}{M_2} \tag{3.14}$$

Eq. (3.14) shows that the target atom, which has zero velocity before the collision in the laboratory reference frame, has the system velocity, $\mathbf{v_c}$, before and after the collision in the CM reference frame.

Eqs. (3.13) and (3.14) show the advantage of the CM reference frame. The system velocity, $\mathbf{v_c}$, and the atom and ion velocities, $\mathbf{v_{atom}}$ and $\mathbf{v_{ion}}$, remain constant and are independent of the final scattering

angle between the two particles (Fig. 3.3(b)). Thus, regardless of whether the collision is elastic or inelastic, the total momentum is unchanged in a collision. In addition, from Eqs. (3.13) and (3.14), we see that the ratio of the ion to atom velocities is inversely proportional to the ratio of their masses:

$$\frac{\mathbf{v_{ion}}}{\mathbf{v_{atom}}} = \frac{\mathbf{v_0} - \mathbf{v_c}}{\mathbf{v_c}} = \frac{M_2}{M_1} = \frac{1}{\mu} \tag{3.15}$$

Another advantage to the CM reference frame is that the CM total energy, E_c, is equal to the CM initial kinetic energy:

$$E_c = \tfrac{1}{2}M_c v_0^2 \tag{3.16a}$$

$$E_c = \frac{1}{2}\frac{M_1 M_2}{M_1 + M_2}v_0^2 = \frac{M_2}{M_1 + M_2}E_0 \tag{3.16b}$$

where $M_1 v_0^2/2 = E_0$.

In our discussion of ion–solid interactions, we will, for the sake of simplicity, carry out many calculations in the center-of-mass system, but we will want to relate the results to experiments in the laboratory. Thus, it is useful to know some of the conversions between variables in these systems.

The conversion of scattering angles from the laboratory system to the CM system is determined from the scattering diagrams given in Fig. 3.3. Examining the target atom (M_2) trajectory portion of Fig. 3.3(a), we see that the final target velocity in the laboratory, $\mathbf{v_2}$, is related to the CM atom velocity, $\mathbf{v_{atom}} = \mathbf{v_c}$, by the difference vector, $\mathbf{v_c}$. Since the triangle formed by these velocity vectors is isosceles, we have

$$\phi_c = 2\phi \tag{3.17}$$

From the CM diagram, Fig. 3.3, we have $\theta_c + \phi_c = \pi$, which allows us to rewrite Eq. (3.17) in the form

$$\phi = \frac{\pi - \theta_c}{2} \tag{3.18}$$

which relates the target atom scattering angle in the laboratory to the CM ion scattering angle.

Another important relationship that will be needed in future discussions on ion stopping and radiation damage is the one between the energy transferred to the target atom as a function of the target atom scattering angle θ_c or θ. Again, from the velocity vector diagram in Fig. 3.3(a), and the law of cosines, we have

$$v_2^2 = v_c^2 + [v_c^2 - 2v_c^2\cos(\pi - \phi_c)] \tag{3.19}$$

Using Eqs. (3.17) and (3.18) to recast ϕ_c in terms of θ_c, we obtain

$$v_2^2 = 2v_c^2(1 - \cos\theta_c) \tag{3.20}$$

which relates the target atom recoil velocity in the laboratory to the CM velocity and the CM ion scattering angle. Eq. (3.20) can be simplified by using Eqs. (3.14) and (3.17) to obtain

$$v_2 = 2v_0\frac{M_c}{M_2}\cos\phi \tag{3.21}$$

which gives the laboratory recoil velocity, v_2, as a function of the initial ion velocity, v_0, and the laboratory recoil angle. This equation can now be used to obtain the energy transferred to the target atom by the incident ion through the kinetic energy velocity relationship,

$$E_2 = \tfrac{1}{2}M_2v_2^2 \tag{3.22}$$

In many books, the energy *transferred* to the target atom, E_2, is referred to as T. Substituting Eq. (3.21) into Eq. (3.22) gives

$$T \equiv E_2 = \frac{M_2}{2}\left(\frac{v_0M_c\cos\phi}{M_2}\right)^2 \tag{3.23}$$

The transferred energy, T, can be related to the ion scattering angle, θ_c, by Eq. (3.18) to yield

$$T = \frac{2}{M_2}\left(v_0M_c\sin\frac{\theta_c}{2}\right)^2 = \frac{4E_cM_c}{M_1}\sin^2\frac{\theta_c}{2} \tag{3.24}$$

From the description of reduced mass, Eq. (3.11), we rewrite Eq. (3.24) to obtain

$$T = E_0\frac{4M_1M_2}{(M_1 + M_2)^2}\sin^2\frac{\theta_c}{2} \tag{3.25}$$

or

$$T = T_M\sin^2\frac{\theta_c}{2} \tag{3.26}$$

where T_M is the maximum energy transferable in a head-on collision, $\theta_c = 0$, and is given by

$$T_M = \frac{4M_1M_2}{(M_1 + M_2)^2}E_0 = \gamma E_0 \tag{3.27}$$

where $\gamma = 4M_1M_2/(M_1 + M_2)^2$. Examining Eq. (3.27) we see that, for the equal mass case, all the energy may be transferred, whereas, for a larger mismatch in particle masses, only a fraction of the energy may be transferred in an elastic collision.

These final relationships give the energy loss by the ion through

Table 3.3. *Energy transfer and angular range of* θ_c

Heavy target	$M_1 \ll M_2$ $0 \leq \lvert\theta_c\rvert < \pi$	$\frac{T}{E_0} \cong \frac{2}{\pi}(1 - \cos\theta_c)$
Equal masses	$M_1 = M_2$ $0 \leq \lvert\theta_c\rvert < \frac{\pi}{2}$	$\frac{T}{E_0} = \sin^2\theta_c$
Light target	$M_1 \gg M_2$ $0 \leq \lvert\theta_c\rvert \leq \tan^{-1}(M_2/M_1) < \frac{\pi}{2}$	$\frac{T}{E_0} \cong \frac{M_1}{M_2}\theta_c^2$

After Johnson (1982).

elastic collisions with target atoms; they will be needed in the development of the concepts of energy-loss cross-section and nuclear stopping which will be discussed in Chapters 4 and 5, respectively.

As an example, to determine the energy transferred in a binary collision where a 100 keV boron ($M_1 = 10$) ion incident on Si ($M_2 = 28$) and scattered through a laboratory angle $\theta = 45°$, one first determines the corresponding CM angle θ_c from the expression given in Table 3.2, $\theta_c = \theta + \sin^{-1}(\mu\sin\theta)$, which gives $\theta_c = 60°$. Next we calculate the ratio T_M/E from Eq. (3.25) which gives $T_M = 0.78E_0$. Finally, for $E_0 = 100$ keV, $T = 19.5$ keV from Eq. (3.26).

Additional relationships between the CM and the laboratory reference frames are summarized in Table 3.2. A summary of the angular range of θ_c and the limitation on transferred energy as a function of M_1/M_2 are presented in Table 3.3. The limitations on laboratory scattering angles are discussed in detail in Appendix E.

3.5 Motion under a central force

In our discussions of ion–solid interactions, we restrict ourselves to central forces, where the potential V is a function of r only, $V = V(r)$, so that the force is always along r. We need consider only the problem of a single particle of mass M_c, moving about a fixed center of force, which will be taken as the origin of the coordinate system. Since potential energy involves only the radial distance, the problem has spherical symmetry, indicating that any rotation about a fixed axis can have no effect on the solution; that is, if either particle is located at the origin, the force on the other is given by a central force $F(r)$, which only depends on the separation distance r.

In the problem examined in this section we will assume that, in the laboratory system, one of the particles is practically at rest at the origin, O, while the other one moves with velocity v, a good approximation when the stationary particle is much heavier than the moving particle.

3.5.1 Conservation of angular momentum

Consider a particle located in space at point P, a distance $\mathbf{r}$ away from a central force originating at point O (Fig. 3.4). If the particle of mass M at P is acted on by a force $\mathbf{F}$, we have

$$\mathbf{F} = M\mathbf{a} = M\frac{d\mathbf{v}}{dt}$$

Forming the vector cross product of the position vector $\mathbf{r}$ with both sides of this equation gives

$$\mathbf{r} \times \mathbf{F} = \mathbf{r} \times M\frac{d\mathbf{v}}{dt} \tag{3.28}$$

The left-hand side of this equation, $\mathbf{r} \times \mathbf{F}$, is the torque $\boldsymbol{\tau}$ due to $\mathbf{F}$

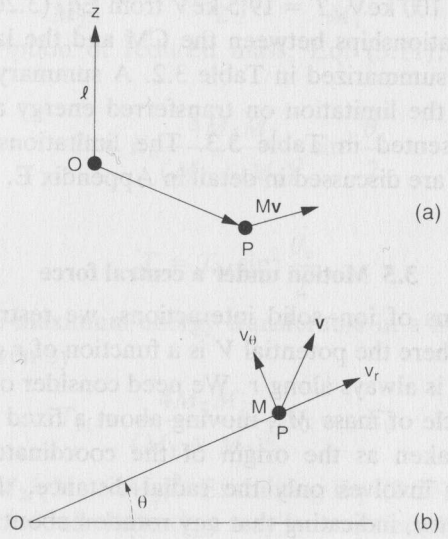

Fig. 3.4. (a) Vector relationship of position, linear momentum, and orbital momentum. (b) Analysis of the velocity into radial and transverse components. (After French, 1971.)

about O. The angular momentum, l, of the particle with respect to the origin is given by

$$l = \mathbf{r} \times M\mathbf{v} = \mathbf{r} \times \mathbf{p} \tag{3.29}$$

The angular momentum l is a vector perpendicular to the plane defined by $\mathbf{r}$ and $\mathbf{v}$ in Fig. 3.4(a), and bears the same relation to linear momentum, $\mathbf{p}$, as torque, $\boldsymbol{\tau}$, does to force, $\mathbf{F}$.

The time rate of change of l is given by

$$\frac{dl}{dt} = \frac{d\mathbf{r}}{dt} \times M\mathbf{v} + \mathbf{r} \times M\frac{d\mathbf{v}}{dt}$$

$$= \mathbf{v} \times M\mathbf{v} + \mathbf{r} \times M\frac{d\mathbf{v}}{dt}$$

From Fig. 3.4, we see that the value of $\mathbf{v} \times M\mathbf{v}$ is zero because it is the cross product of two parallel vectors. The second term is simply the torque due to the force about O, Eq. (3.28), leading to the expression

$$\boldsymbol{\tau} = \mathbf{r} \times \mathbf{F} = \frac{dl}{dt} \tag{3.30}$$

Eq. (3.30) relates the torque to the time rate of change of the orbital angular momentum of the particle about the origin O. For $\mathbf{F} = \mathbf{F}(\mathbf{r})$, a central force, which is directed radially away or toward O, $\mathbf{F}$ is parallel to $\mathbf{r}$ and $\boldsymbol{\tau} = \mathbf{F} \times \mathbf{r} = 0$. Thus, for a central force we have

$$\frac{dl}{dt} = 0 \tag{3.31}$$

which, when applied to Eq. (3.29), gives

$$l = \mathbf{r} \times \mathbf{p} = \text{constant} \tag{3.32}$$

Eq. (3.32) is the statement of the conservation of orbital angular momentum for the motion of mass M under a central force.

If we examine the situation described by Fig. 3.4(a) in the plane of motion, which is defined by vectors $\mathbf{r}$ and $\mathbf{v}$, the problem can be presented in polar coordinates, and the velocity can be broken down into its radial, v_r, and transverse, v_θ coordinates, Fig. 3.4(b). For the polar representation in Fig. 3.4(b), the vector l points out of the page, and its magnitude is given by

$$l = rMv_\theta = Mr^2\frac{d\theta}{dt} \tag{3.33}$$

where the product $rv_\theta = r^2\,d\theta/dt$ is constant for a central force. For ion–solid interactions and a CM coordinate system, M in Eq. (3.33) is replaced by M_c.

3.5.2 Energy conservation in a central force

For conservative central forces and a defined interaction potential, $V(r)$, we can write a statement for the total mechanical energy for a particle of mass M, a distance r away from a central force, F, as defined in Fig. 3.4(b), as

$$E = \frac{M}{2}[v_r^2 + v_\theta^2] + V(r) \tag{3.34}$$

where v_r and v_θ are the radial and transverse velocities, respectively. The first term on the right-hand side of Eq. (3.34) represents the kinetic energy in polar coordinates.

In addition to the total energy equation given above, we also have the condition of conservation of angular momentum given in Eq. (3.33)

$$l = Mrv_\theta$$

The quantities E and l are the constants of motion, while $V(r)$ is the potential energy for a particle of mass M in a central field. Eqs. (3.33) and (3.34) allow us to reduce the three-dimensional problem described in Fig. 3.4(a) to a one-dimensional problem, Fig. 3.4(b), an advantage of central field formulation.

Using Eq. (3.33) we rewrite Eq. (3.34) in the form

$$E = E(r) = \frac{Mv_r^2}{2} + \frac{l^2}{2Mr^2} + V(r) \tag{3.35}$$

All terms in Eq. (3.35) are a function of r only: the first term is the kinetic energy for the radial component, the term $l^2/2Mr^2$ is referred to as the *centrifugal energy*, and $V(r)$ is the interatomic potential energy. The centrifugal energy is the portion of the kinetic energy term which is due to the particle's motion transverse to the direction of the radius vector. It is because the centrifugal energy can be described as a function of radial position r alone that we can treat the radial motion of a particle as a one-dimensional problem in r. Eq. 3.35 is now simply a function of r only.

3.5.3 Angular orbital momentum and the impact parameter

Consider an interaction potential energy, $V(r)$, that tends to zero as r approaches infinity. This situation corresponds to the condition that a moving particle has positive kinetic energy at infinity. If $V(r)$ is everywhere positive, but decreasing monotonically with r, the potential is repulsive, and the radial motion of this particle in the field $V(r)$ will have no bounds or limits in its maximum value of r. However, there is a minimum in r, the *distance of closest approach*, r_{min}, that depends on the particle's total energy and the nature of the interaction potential.

In Fig. 3.5(a), the energy curves for attractive and repulsive potential energy, differing only in sign, are presented along with an arbitrarily defined centrifugal energy curve. In Fig. 3.5(b), the effective potential energy curves

$$V'(r) = V(r) + \frac{l^2}{2Mr^2} \tag{3.36}$$

are shown for the two cases. Fig. 3.6 gives a schematic representation of how the effective potential energy affects the trajectories of a particle moving with an energy $E = Mv^2/2$. The distance of closest approach is determined by the value of r that satisfies the condition $E = V'(r)$.

At large distances away from the center of force, the magnitudes of $V(r)$ and $l^2/2Mr^2$ will be negligible; see Fig. 3.6. Under such conditions, a particle with energy E travels in a straight line with a speed $v_0 = (2E/M)^{1/2}$. The particle's direction of motion is offset from a parallel line through the center of force (target atom) by a distance b that is directly related to the centrifugal energy and the angular orbital

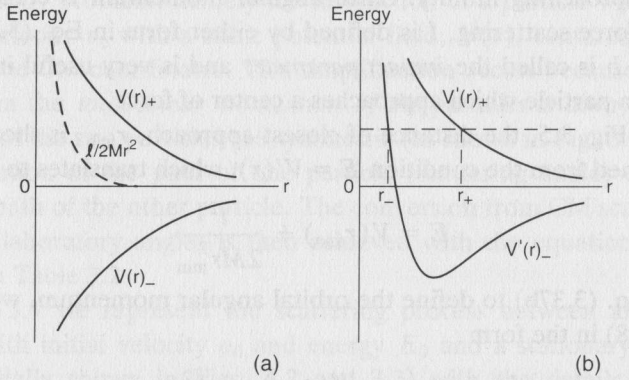

Fig. 3.5. (a) Centrifugal potential-energy curve (dashed) and two potential-energy curves, differing only in sign, that might arise from electrical interactions of like and unlike charges. (b) Effective potential-energy curves corresponding to the two cases shown in (a), indicating different distances of closest approach for a given positive total energy. (After French, 1971.)

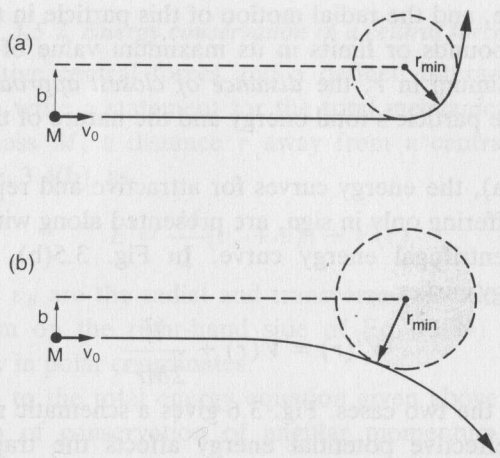

Fig. 3.6. (a) Plan view of trajectory of a particle moving around a center of attraction. The angular momentum is defined by the *impact parameter*, b. (b) Corresponding trajectory with the same impact parameter, but with a repulsive center of force. (After French, 1971.)

momentum. From the law of conservation of angular momentum,

$$l = Mr_{\min}v_\theta \tag{3.37a}$$

approaches

$$l = Mv_0 b \tag{3.37b}$$

for r approaching infinity. Since angular momentum is conserved in central force scattering, l is defined by either form in Eq. (3.37). The distance b is called the *impact parameter* and is very useful in characterizing a particle which approaches a center of force.

From Fig. 3.5, the distance of closest approach, $r_{\min}$, is shown to be determined from the condition $E = V'(r)$, which translates to

$$E = V(r_{\min}) + \frac{l^2}{2Mr_{\min}^2} \tag{3.38}$$

Using Eq. (3.37b) to define the orbital angular momentum, we rewrite Eq. (3.38) in the form

$$0 = 1 - \frac{V(r_{\min})}{E} - \frac{b^2}{r_{\min}^2} \tag{3.39}$$

where $E = E_c$ in the CM system. Eq. (3.38) shows that $r_{\min}$ will depend on the energy of the ion and the form of the interatomic potential. Knowledge of $V(r)$ allows one to find $r_{\min}$ by applying the quadratic equation to Eq. (3.39).

3.6 The classical scattering integral

In this section, we will derive an expression for the CM scattering angle θ_c. We will see that θ_c will depend on the interatomic potential $V(r)$, the ion energy E, and the impact parameter b.

The discussions in Sections 3.3–3.4 of this chapter have reviewed the elastic scattering process for the two-particle systems by only considering the asymptotic values of momentum and energy at distances far from the collision site. However, to proceed with the development of ion–solid interactions, we must know the probability for each scattering angle, which will allow us to determine the energy transferred during scattering. The probability for a given scattering angle will lead to the concept of the energy transfer cross-section in Chapter 4. The only way to determine the probability of each scattering angle is by evaluating the details of the scattering trajectory, which requires us to understand the motion of the particles under a central force.

As we showed in Section 3.5, the problem of defining the scattering trajectory of a moving particle in a central force field is greatly simplified by assuming that the force between the two particles acts only along the line joining them, and that there are no transverse forces. The use of CM coordinates then reduces any two-body problem to a one-body problem, namely the interaction of a particle with mass M_c and velocity v_c with a static potential field, $V(r)$, centered at the origin of the CM coordinates. This simplification occurs because in the CM system the *total linear momentum of the particles is always zero*, the paths of the two particles are symmetric (as shown in Fig. 3.3), and the evaluation of the path of one particle (scattering angle) directly gives the path of the other particle. The conversion from CM scattering angles to laboratory angles is then achieved with the equations summarized in Table 3.2.

In Fig. 3.7 we represent the scattering process between an atom moving with initial velocity v_0 and energy E_0 and a stationary target atom (initially shown in Figs. 3.2 and 3.3) with the details of the scattering trajectories displayed for both the laboratory and the CM reference frames. The distance b in the figure is the impact parameter, as discussed in Section 3.5.3, and defines the length of the perpendicular between the initial position of the target atom and the incident

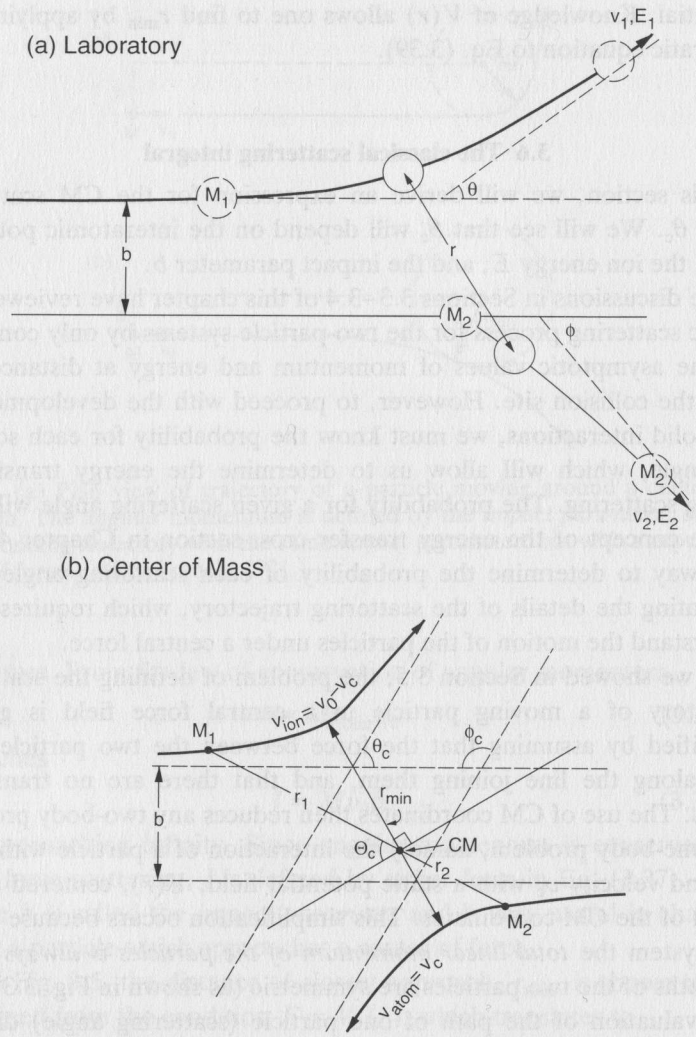

Fig. 3.7. The collision trajectories at an impact parameter b for an elastic collision between two unequal masses, as seen in the (a) laboratory reference frame and (b) CM reference frame.

trajectory of the ion. This parameter will be shown to be an important quantity in the scattering process and will define the hardness of the collision. The dashed lines in Fig. 3.7 represent the asymptotes of the ion and target atom trajectories. The parameter $r_{\min}$ is the distance of closest approach during the scattering event.

Since we are dealing with two particles only and no transverse forces, the problem is two-dimensional in the plane defined by the initial velocity vector for the ion and the initial position of the target atom. Since we are dealing with conservative central forces, defined by an ion–atom interaction potential $V(r)$, conservation of energy in the center-of-mass system will be

$$E_c = \tfrac{1}{2}M_c(\dot{\mathbf{r}}^2 + \mathbf{r}^2\dot{\boldsymbol{\Theta}}_c^2) + V(r) \tag{3.40}$$

where the first term is the system kinetic energy. The variable r is defined in Fig. 3.7 as

$$r = r_1 + r_2 \tag{3.41}$$

with the CM distances r_1 and r_2 defined by

$$r_1 = \frac{M_2}{M_1 + M_2}r \tag{3.42a}$$

$$r_2 = \frac{M_1}{M_1 + M_2}r \tag{3.42b}$$

The variable r is the CM separation distance between M_1 and M_2, and r_1 and r_2 represent the distance from the center of mass to the ion (M_1) and the target atom (M_2), respectively. The value $\dot{\boldsymbol{\Theta}}_c$ is the time rate of change in the scattering angle, $d\boldsymbol{\Theta}_c/dt$, and $\boldsymbol{\Theta}_c$ is defined as the angle between line $r_1 + r_2$ and the line perpendicular to $r_{\min}$ and is different from the CM scattering angle θ_c. The energy E_c is the CM energy, defined in Eq. (3.16), and M_c is the CM mass, defined in Eq. (3.11).

In addition to the conservation of energy, we have the law of conservation of angular momentum, Eq. (3.33), which, during the scattering process in the CM system, is given by

$$l = M_c r^2\dot{\boldsymbol{\Theta}}_c \tag{3.43}$$

where l is the constant angular momentum. For large values of r, the angular momentum is simply related to the impact parameter and has the magnitude $M_c v_0 b$ (Eq. (3.37)). Since angular momentum is conserved we have

$$l = M_c r^2\dot{\boldsymbol{\Theta}}_c = M_c v_0 b \tag{3.44}$$

from which we obtain

$$\dot{\boldsymbol{\Theta}}_c = \frac{v_0 b}{r^2} \tag{3.45}$$

With Eqs. (3.40), (3.44), and (3.45), we can now solve for $\boldsymbol{\Theta}_c$ as a

function of any central force potential, $V(r)$. From these equations we obtain the radial equation of motion

$$\dot{r} = v_0\left(1 - \frac{V(r)}{E_c} - \left(\frac{b}{r}\right)^2\right)^{1/2} \tag{3.46}$$

Using this result and noting that $\dot{r} = (dr/dt)$ and that $\dot{\Theta}_c = (d\dot{\Theta}_c/dt)$, we obtain

$$\frac{d\Theta_c}{dt} \cdot \frac{dt}{dr} = \frac{d\Theta_c}{dr} = \frac{b}{r^2\left[1 - \frac{V(r)}{E_c} - \left(\frac{b}{r}\right)^2\right]^{1/2}} \tag{3.47}$$

The CM scattering angle θ_c is found by integrating Θ_c on the left-hand side of Eq. (3.47) over the first half of the orbit, from $\theta_c/2$ to $\pi/2$, which corresponds to the integration limits on the right-hand side of r_{min} to infinity:

$$\int_{\theta_c/2}^{\pi/2} d\Theta_c = \int_{r_{min}}^{\infty} \frac{b\,dr}{r^2\left[1 - \frac{V(r)}{E_c} - \left(\frac{b}{r}\right)^2\right]^{1/2}} \tag{3.48}$$

$$\tfrac{1}{2}(\pi - \theta_c) = \int_{r_{min}}^{\infty} \frac{b\,dr}{r^2\left[1 - \frac{V(r)}{E_c} - \left(\frac{b}{r}\right)^2\right]^{1/2}} \tag{3.49}$$

which reduces to

$$\theta_c = \pi - 2b\int_{r_{min}}^{\infty} \frac{dr}{r^2\left[1 - \frac{V(r)}{E_c} - \left(\frac{b}{r}\right)^2\right]^{1/2}} \tag{3.50}$$

This final equation is called the *classical scattering integral* and gives the angular trajectory information for two-body central force scattering. Eq. (3.50) allows us to evaluate the scattering angle θ_c in terms of energy E_c, the interatomic potential $V(r)$, and the impact parameter b. The scattering angle of an ion with energy E, moving in a force field defined by V(r), will vary with the impact parameter b. The significance of this will become clear when we discuss the differential scattering cross-section in Chapter 4, where Eq. (3.50) is solved explicitly for a Coulomb potential. In general, potentials are more complex and numerical solutions are required. Transformations from the CM angle θ_c to the laboratory angles θ and ϕ can be made with the help of Table 3.2.

A comparison of Eqs. (3.50) and (3.39) shows that the distance of closest approach, r_{min}, can be found by setting the expression under the radical in Eq. (3.50) to zero. Since the radical in Eq. (3.50) is zero at $r = r_{min}$, Eq. (3.50) has a singularity at $r = r_{min}$, which must be avoided during the integration processes. This can be accomplished by carrying out the following substitution:

$$u = \frac{1}{r} \tag{3.51}$$

With this change of variables, the integration limits are transformed to $1/\infty = 0$ and $1/r_{min}$, which transforms Eq. (3.50) to

$$\theta_c = \pi - 2b\int_0^{1/r_{min}} \frac{du}{\left[1 - \frac{V(u)}{E_c} - (bu)^2\right]^{1/2}} \tag{3.52}$$

This final form of the scattering integral removes the singularity as u tends to zero.

3.7 Distance of closest approach

The distance of closest approach was defined by Eq. (3.39) and can be rewritten as

$$\frac{V(r_{min})}{1 - b^2/r_{min}^2} = E_c = \frac{M_2}{M_1 + M_2}E_0 \tag{3.53}$$

where Eq. (3.16) was used to transform the CM energy E_c to the laboratory energy E_0. For a Coulomb potential, Eq. (2.4), and a *head-on collision*, $b = 0$, we can rewrite Eq. (3.53) as

$$d_c \equiv (r_{min})_{b=0} = \frac{M_1 + M_2}{M_2 E_0} Z_1 Z_2 e^2 = \frac{Z_1 Z_2 e^2}{E_c} \tag{3.54}$$

For a head-on collision, $r_{min} \equiv d_c$, where d_c is called the *collision diameter*. For a given interatomic potential and ion energy, the collision diameter gives the lower limit to r_{min}.

As an example, for 1 MeV He ($Z_1 = 2$) ions incident on Si ($Z_2 = 14$), the CM energy $E_c = M_2E_0/(M_1 + M_2) = 875$ keV and the distance of closest approach, the collision diameter $= Z_1Z_2e^2/E_c = 4.6 \times 10^{-5}$ nm, a value much smaller than a_{TF}. It is informative to write d_c relative to the screening distance a_{TF}, where the parameter a_{TF}/d_c is referred to as ε, the reduced energy, given by

$$\varepsilon \equiv \frac{a_{TF}}{d_c} = \frac{a_{TF}E_c}{Z_1Z_2e^2} = \frac{E}{Z_1Z_2e^2}\frac{a_{TF}M_2}{M_1 + M_2} \tag{3.55}$$

Examining Eq. (3.55) we see that ε is a dimensionless energy unit. Physically, ε gives a measure of how energetic the collision is and how close the ion gets to the nucleus of the target atom. For example, the value of the Thomas–Fermi screening distance a_{TF} for He on Si is

$$a_{TF} = \frac{0.885 \times 0.053}{(Z_1^{1/2} + Z_2^{1/2})^{2/3}} = 1.5 \times 10^{-2} \text{ nm}$$

The reduced energy for 1 MeV He ions is

$$\varepsilon = \frac{a_{TF}}{d_c} = \frac{1.5 \times 10^{-2}}{4.6 \times 10^{-5} \text{ nm}} = 3.4 \times 10^3$$

This large value of ε is consistent with the very small value of the collision diameter.

For calculation purposes, Eq. (3.55) can be simplified and rewritten as

$$\varepsilon = \frac{0.03255\ E(\text{eV})}{Z_1 Z_2 (Z_1^{2/3} + Z_2^{2/3})^{1/2}} \frac{M_2}{M_1 + M_2} \tag{3.56}$$

References

French, A. P. (1971) *Newtonian Mechanics* (W. W. Norton & Co., New York).

Johnson, R. E. (1982) *Introduction to Atomic and Molecular Collisions* (Plenum Press, New York).

Sigmund, P. (1972) Collision Theory of Displacement Damage, Ion Ranges and Sputtering, *Rev. Roumaine Phys.* **17**, pp. 823, 969 & 1079.

Weller, R. (1995) in *Handbook of Modern Ion-Beam Materials Analysis*, eds. J. R. Tesmer and M. Nastasi (Materials Research Society, Pittsburgh, PA), 1995.

Suggested reading

Classical Mechanics, H. Goldstein (Addison-Wesley Publishing Co., Reading, Mass., 1959).

Defects and Radiation Damage in Metals, M. W. Thompson (Cambridge University Press, 1969).

Fundamental Aspects of Nuclear Reactor Fuel Elements, D. R. Olander (National Technical Information Service, Springfield, Virginia, 1976), chap. 17.

Fundamentals of Surface and Thin Film Analyses, L. C. Feldman and J. W. Mayer (North-Holland Science Publishing, New York, 1986).

Interatomic Potentials, I. M. Torrens (Academic Press, New York, 1972).

Mechanics, K. R. Symon (Addison-Wesley Publishing Co., Reading, Mass., 1953).

The Stopping and Range of Ions in Solids, J. F. Ziegler, J. P. Biersack, and U. Littmark (Pergamon Press Inc., New York, 1985).

Problems

3.1 Derive the expression for the laboratory energy of the recoil nucleus as written in Table 3.2.

3.2 Write a simple expression for E_1/E_0 and E_2/E_0 in backscattering ($\theta = 0$) and right-angle scattering ($\theta = 90°$) for $M_1 = M_2$, $M_1 > M_2$, and $M_1 < M_2$. What are the allowed solutions?

3.3 What is the maximum energy transferred to electrons, silicon atoms, and copper atoms by incident 100 keV electrons, silicon ions, and copper ions?

3.4 In the laboratory system, we have arsenic ions at 100 keV scattered from silicon atoms at $\theta = 10°$.
(a) In the laboratory system, what is v_1, v_2, ϕ, and E_2?
(b) In the center-of-mass system, what is v_{ion}, θ_c, and ϕ_c?

3.5 Solve the scattering integral, Eq. (3.52), for the unscreened Coulomb potential $V(r) = Z_1 Z_2 e^2/r$.
(a) Derive a general expression for the distance of closest approach, r_{min}, for the unscreened potential.
(b) What is the value of r_{min} for 2 MeV ^{4}He incident on gold for a head-on collision, $b = 0$, and for $b = 0.5a_L$ and $5a_L$, where a_L is defined in Eq. (2.47).

3.6 Prove that $l = Mrv_\theta$ approaches $l = Mv_0 b$ for r approaching infinity (Eq. (3.37)).

3.7 Using Eq. (3.39) and assuming a pure Coulomb potential, calculate the value of r_{min} for a 100 keV boron atom ($Z_1 = 5$) on silicon ($Z_2 = 14$) for an impact parameter $b = 1$ nm. What is the significance of your answer?

4
Cross-section

4.1 Introduction

In Chapters 2 and 3 we developed concepts essential to our understanding of ion–solid interactions. In Chapter 3 we derived equations describing the kinematics of binary elastic collisions. These equations enable us to calculate the amount of energy transferred to a target atom in a collision when the scattering angle of the projectile or the target atom is known. Conversely, we could calculate the scattering angles if the amount of energy loss in the collision were known. At the end of Chapter 3 we developed an expression for the center-of-mass scattering angle, θ_c, which is a function of the ion energy, the impact parameter b, and the interatomic potential energy $V(r)$. The details of the interatomic potential energy were discussed in Chapter 2.

In Chapter 4 we will examine the probability of ion–solid scattering events. During ion irradiation and ion implantation experiments, many ions or energetic particles interact with many target nuclei. Due to the large number of interactions, the questions of how much energy will be transferred in a collision or what the scattering angle will be must be answered using statistics and probability. The differential cross-section is the fundamental parameter that we will develop. It gives a measure of either the probability of transferring energy T in the range between T and $T + dT$ to a target atom or of the probability of scattering a projectile into some angle between θ_c and $\theta_c + d\theta_c$. The differential cross-section has units of area, typically centimeters squared. The differential cross-section integrated over all angles is the total cross-section, often referred to simply as the cross-section.

The differential cross-section will become an important parameter in describing ion ranges in solids and radiation damage, both of which will be discussed later in this book. The differential cross-section depends strongly on the form of the interatomic potential.

4.2 Angular differential scattering cross-section

In ion–solid interactions, it is customary to describe the number of particles scattered through different angles θ_c in terms of a quantity called the angular differential scattering cross-section. Imagine the experiment depicted in Fig. 4.1, where a beam of ions is incident on a thin foil and is scattered into a detector of area Δa at a polar angle between θ_c and $\theta_c + d\theta_c$. Each of the ions in the incident beam has a different impact parameter b (as described in Chapter 3) and will be scattered through a different angle. We define the differential dn_θ as the number of ions scattered into the detector of area Δa, between angles θ_c and $\theta_c + d\theta_c$, per unit time. We also define I_0 to be the flux of incident particles, equal to the number of ions incident on the sample per unit time, per unit area (i.e., ions per second per centimeter squared). The solid angle of the detector, $\Delta\Omega$, is related to the detector area, Δa, and its distance away from the sample, R, and is given by

$$\Delta\Omega = \frac{\Delta a}{R^2} = \frac{(R\Delta\theta_c)(R\sin\theta_c\Delta\varphi)}{R^2} = \Delta\theta\Delta\varphi\sin\theta_c \qquad (4.1)$$

We now define $d\sigma(\theta_c)$, the differential scattering cross-section, to be

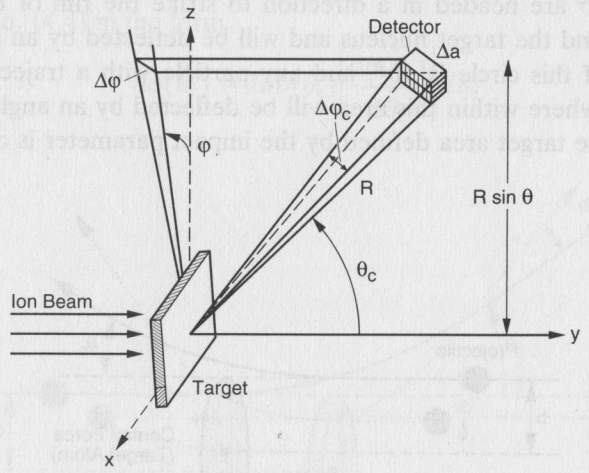

Fig. 4.1. Experiment for measuring angular differential cross-section. The detector area is $\Delta a = (R\Delta\theta_c)(R\sin\theta_c\Delta\varphi)$. By moving the detector to all angular positions for a fixed R, all the scattered particles can be counted, and the detector will have covered an area $4\pi R^2$, or a total solid angle of 4π.

given by

$$\frac{d\sigma(\theta_c)}{d\Omega} \equiv \frac{1}{I_0}\frac{dn_\theta}{d\Omega} \tag{4.2}$$

where for $\Delta a \to 0$ we have $\Delta\Omega \to d\Omega$. The term $d\sigma(\theta_c)/d\Omega$ is the differential scattering cross-section per unit solid angle, and $dn_\theta/d\Omega$ is the number of particles scattered into the angular regime between θ_c and $\theta_c + d\theta_c$ per unit solid angle. Since the units of Ω (steradian) are dimensionless, the differential scattering cross-section has units of area.

The cross-section is simply the effective target area presented by each scattering center (target nucleus) to the incident beam. At a more microscopic level, the scattering cross-section can be shown to be dependent on b, the impact parameter. In Fig. 4.2 we present the collision process in which the incident particle is scattered by a target nucleus through an angle θ_c. The projectile moves in a nearly straight line until it gets fairly close to the target nucleus, at which point it is deflected through an angle θ_c. After being deflected, the trajectory of the particle is again nearly a straight line. If there had been no interaction force between the projectile and the target nucleus, the projectile would have maintained a straight trajectory and passed the target nucleus at a distance b.

On examining Fig. 4.2, we see that all incident particles with impact parameter b are headed in a direction to strike the rim of the circle drawn around the target nucleus and will be deflected by an angle θ_c. The area of this circle is πb^2, and any particle with a trajectory that strikes anywhere within this area will be deflected by an angle greater than θ_c. The target area defined by the impact parameter is called the

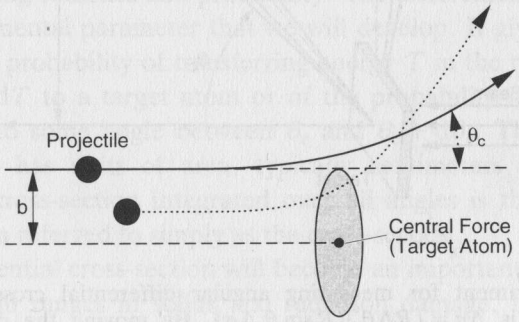

Fig. 4.2. Scattering of a particle that approaches a nucleus with an impact parameter b. The total cross-section is $\sigma = \pi b^2$.

total cross-section $\sigma(\theta_c)$:

$$\sigma(\theta_c) = \pi b^2 \tag{4.3}$$

For projectiles moving with small values of b, the cross-section defined by Eq. (4.3) will be small, but, due to the interaction forces, the scattering angle will be large. Thus, b is proportional to $\sigma(\theta_c)$, while I_0 and $\sigma(\theta_c)$ are inversely related to θ_c. From this discussion, we see that $b = b(\theta_c)$.

In addition to the total cross-section, there is the differential cross-section, $d\sigma(\theta_c)$, and its relationship to b. As shown in Fig. 4.3, particles incident with impact parameters between b and $b + db$ will be scattered through angles between θ_c and $\theta_c + d\theta_c$. The differential cross-section for this process is found by taking the differential of Eq. (4.3) with respect to the impact parameter:

$$d\sigma(\theta_c) = d(\pi b^2) = 2\pi b\, db \tag{4.4}$$

From the description given in Eq. (4.4) and the schematic presented in Fig. 4.3, the differential cross-section of each target nucleus is presented as a ring of radius b, a circumference $2\pi b$, and width db. Any incident particles with an impact parameter within db will be scattered into angles between θ_c and $\theta_c + d\theta_c$.

From the examples presented in Figs. 4.2 and 4.3, we see that there is a unique connection between the value of b and the scattering angle θ_c. To find the dependence of $d\sigma(\theta_c)$ on the scattering angle, we rewrite Eq. (4.4) in the form

$$d\sigma(\theta_c) = 2\pi b(\theta_c)\left|\frac{db(\theta_c)}{d\theta_c}\right| d\theta_c \tag{4.5}$$

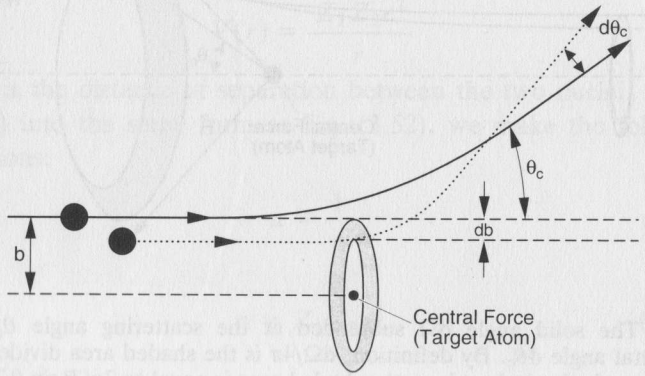

Fig. 4.3. Nuclear target area for the differential cross-section $d\sigma = 2\pi b\, db$.

We use the absolute value of $db(\theta_c)/d\theta_c$ to maintain $d\sigma(\theta_c)$ as a positive value; θ_c increases as b decreases, indicating that $db(\theta_c)/d\theta_c$ is negative.

To determine an expression for the differential scattering cross-section per unit solid angle (Eq. 4.1), we note that scattering experiments are performed by observing the number of incident particles that are scattered into a solid angle located at θ_c. Measurements give information in units of the number of scattering particles per element of solid angle. A schematic of this process is presented in Fig. 4.4. The annular region represents the solid angle $d\Omega$ subtended between the scattering angles θ_c and $\theta_c + d\theta_c$. The entire area of the sphere of radius R is $4\pi R^2$, and the total solid angle of the sphere is 4π. The shaded area is a ring of radius $R \sin\theta_c$, circumference $2\pi R \sin\theta_c$, and width $R d\theta_c$. The area of the shaded ring is therefore $(2\pi)(R\sin\theta_c)(R d\theta_c) = 2\pi R^2 \sin\theta_c d\theta_c$. By definition of solid angle, area/R^2, we obtain

$$d\Omega = 2\pi \sin\theta_c \, d\theta_c \tag{4.6}$$

The result is equivalent to Eq. (4.1), where $\Delta\varphi$ has been integrated over 2π. The differential scattering cross-section for scattering into a solid angle $d\Omega$ (Eq. (4.1)) is obtained by combining Eqs. (4.5) and

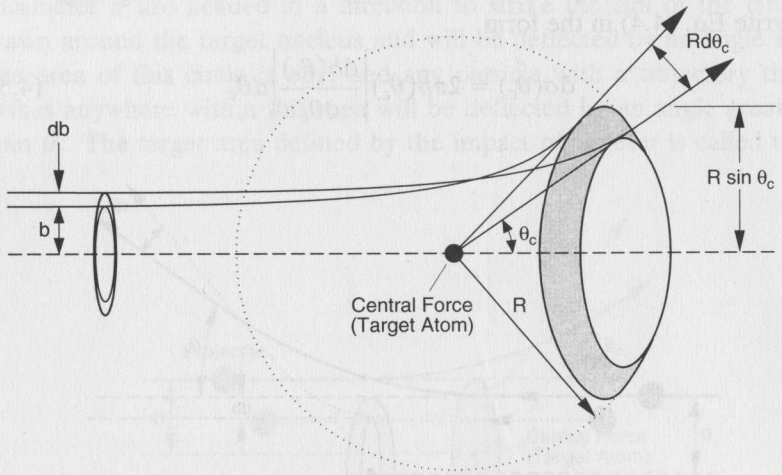

Fig. 4.4. The solid angle $d\Omega$ subtended at the scattering angle θ_c by the incremental angle $d\theta_c$. By definition, $d\Omega/4\pi$ is the shaded area divided by the entire area of spherical surface; the shaded area is equal to $2\pi(R\sin\theta_c)(R\,d\theta_c)$. Then $d\Omega/4\pi = 2\pi R^2 \sin\theta_c \, d\theta_c/4\pi^2$; therefore $d\Omega = 2\pi \sin\theta_c \, d\theta_c$.

(4.6) to produce

$$\frac{d\sigma(\theta_c)}{d\Omega} = \frac{b}{\sin\theta_c}\left|\frac{db}{d\theta_c}\right| \tag{4.7}$$

Eqs. (4.5) and (4.7) give the differential scattering cross-section in the center of mass. The equivalent expressions in the laboratory reference frame can be obtained for the scattered projectile and scattered target nucleus by using the angular relationships presented in Table 3.2.

Integration of Eq. (4.7) provides a relationship between the differential scattering cross-section and the impact parameter:

$$\int_0^b b(\theta_c)\, db = \int_{\theta_c}^{\pi} \frac{d\sigma(\theta_c)}{d\Omega} \sin\theta_c \, d\theta_c$$

which results in the expression

$$b^2 = 2\int_{\theta_c}^{\pi} \frac{d\sigma(\theta_c)}{d\Omega} \sin\theta_c \, d\theta_c \tag{4.8}$$

where the dependence of scattering angles on the impact parameter has been omitted for brevity. By linking Eq. (4.8) with the expression for θ_c (Eq. (3.50)), an effective means of passing between $V(r)$ and $d\sigma(\theta_c)$ can be established.

As an example of the use of the angular differential cross-section, we consider the condition where the interaction between colliding particles is purely Coulombic; for this situation the projectile and target nucleus are treated as pure nuclei, with the projectile described by mass and atomic number M_1 and Z_1, and the target nucleus described by mass and atomic number M_2 and Z_2. The interatomic potential for Coulomb interaction is given by

$$V(r) = \frac{Z_1 Z_2 e^2}{r} \tag{4.9}$$

where r is the distance of separation between the two nuclei. To put Eq. (4.9) into the same form as Eq. (3.52), we make the following substitutions:

$$u \equiv \frac{1}{r} \tag{4.10a}$$

and

$$\alpha = Z_1 Z_2 e^2 \tag{4.10b}$$

leading to

$$V(u) = \alpha u \tag{4.11}$$

With the interatomic potential written in this way, the angular scattering integral (Eq. (3.52)) becomes

$$\theta_c = \pi - 2\int_0^{1/r_{min}} \frac{du}{\left[\frac{1}{b^2} - \frac{\alpha u}{E_c b^2} - u^2\right]^{1/2}} \tag{4.12}$$

Eq. (4.12) can be integrated exactly by noting the following integral solution:

$$\int \frac{dx}{(a + cx + dx^2)^{1/2}} = \frac{-1}{(-d)^{1/2}} \sin^{-1}\left(\frac{c + 2dx}{(q)^{1/2}}\right)$$

where $q = c^2 = 4ad$. For Eq. (4.12), these variables are equal to

$$a = \frac{1}{b^2}; \quad c = \frac{-\alpha}{E_c b^2}; \quad d = -1$$

$$q = \frac{4}{b^2}\left(1 + \frac{\alpha^2}{4E_c^2 b^2}\right)$$

and

$$c + 2dx = -\left(2u + \frac{\alpha}{E_c b^2}\right)$$

After carrying out these substitutions, the solution to Eq. (4.12) is now given by

$$\theta_c = \pi - 2\left[\sin^{-1}\left(\frac{-\left(bu + \frac{\alpha}{2E_c b}\right)}{\left(1 + \frac{\alpha^2}{4E_c^2 b^2}\right)^{1/2}}\right)\right]_0^{1/r_{min}} \tag{4.13}$$

To complete the integration, a value for r_{min} must first be obtained. From the definition of r_{min} given in Eq. (3.39), and using the change in variables defined by Eqs. (4.10) and (4.11), we have

$$b^2 u_{min}^2 + \frac{\alpha u_{min}}{E_c} - 1 = 0 \tag{4.14}$$

where $u_{min} = 1/r_{min}$. Eq. (4.14) is solved for u_{min} using the quadratic equation, and has the solution

$$u_{min} = \frac{1}{r_{min}} = \frac{1}{b}\left(\frac{-\alpha}{2bE_c} \pm \left(\left(\frac{\alpha}{2bE_c}\right)^2 + 1\right)^{1/2}\right) \tag{4.15}$$

Applying Eq. (4.15) to the upper limit in Eq. (4.13) gives

$$\theta_c = \pi - 2\left\{\pm\frac{\pi}{2} - \sin^{-1}\left(\frac{\frac{\alpha}{2E_c b}}{\left(1 + \left(\frac{\alpha}{2E_c b}\right)^2\right)^{1/2}}\right)\right\} \tag{4.16}$$

which can be rewritten as

$$\frac{\theta_c - \pi}{2} = \pm\frac{\pi}{2} + \sin^{-1}\left(\frac{\alpha}{2E_c b}\left[1 + \left(\frac{\alpha}{2E_c b}\right)^2\right]^{-1/2}\right) \tag{4.17}$$

We now use Eq. (4.17) to express b in terms of θ_c. Eq. (4.17) can be rewritten as

$$\sin\left(\frac{\theta_c - \pi}{2} \pm \frac{\pi}{2}\right) = \pm\sin\left(\frac{\theta_c}{2}\right) = \frac{\frac{\alpha}{2E_c b}}{\left[1 + \left(\frac{\alpha}{2E_c b}\right)^2\right]^{1/2}}$$

The trigonometric representation of this equation is presented in Fig. 4.5, which allows us to construct the following relationship between the impact parameter b and the scattering angle θ_c:

$$b = \frac{\alpha}{2E_c}\cot\left(\frac{\theta_c}{2}\right) = \frac{\alpha}{2E_c}\frac{\cos(\theta_c/2)}{\sin(\theta_c/2)} \tag{4.18}$$

We will now use Eq. (4.18) together with Eq. (4.7), $d\sigma(\theta_c)/d\Omega = b/\sin\theta_c|db/d\theta_c|$, to obtain the differential cross-section for scattering

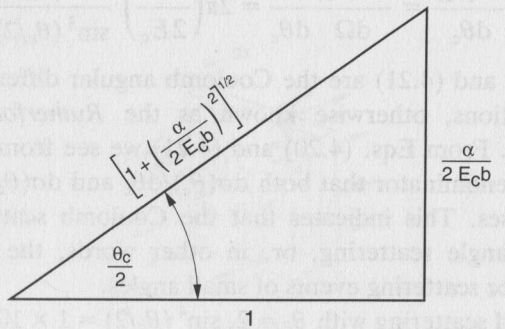

Fig. 4.5. Trigonometric relation between the center-of-mass scattering angle, θ_c, and the impact parameter, b, for the Coulomb potential.

into a solid angle $d\Omega$ for the Coulomb potential. Differentiating Eq. (4.18) with respect to θ_c

$$\frac{db}{d\theta_c} = \frac{\alpha}{2E_c}\frac{d(\cot(\theta_c/2))}{d\theta_c} = \frac{\alpha}{2E_c}\frac{d}{d\theta_c}\left(\frac{\sin(\theta_c/2)}{1-\cos(\theta_c/2)}\right) = \frac{\alpha}{4E_c\sin^2(\theta_c/2)} \tag{4.19a}$$

and multiplying by b

$$b\frac{db}{d\theta_c} = \frac{1}{2}\left(\frac{\alpha}{2E_c}\right)^2\frac{\cot(\theta_c/2)}{\sin^2(\theta_c/2)} \tag{4.19b}$$

leads to

$$\frac{d\sigma(\theta_c)}{d\Omega} = \frac{b}{\sin\theta_c}\left|\frac{db}{d\theta_c}\right| = \frac{1}{2}\left(\frac{\alpha}{2E_c}\right)^2\frac{\cot(\theta_c/2)}{\sin\theta_c\sin^2(\theta_c/2)}$$

or

$$\frac{d\sigma(\theta_c)}{d\Omega} = \left(\frac{\alpha}{4E_c}\right)^2\frac{1}{\sin^4(\theta_c/2)} \tag{4.20}$$

where the geometrical relation $\sin\theta_c = 2\sin(\theta_c/2)\cos(\theta_c/2)$ has been used.

For 1 MeV ^{4}He ions ($Z_1 = 2$) incident on silicon ($Z_2 = 14$), the value of $E_c = 875$ keV and $\alpha = 40.3$ eV nm. For a 180° backscattering event, $\theta_c/2 = 90°$ and $\sin^4(\theta_c/2) = 1$. Then $d\sigma(\theta_c)/d\Omega = (\alpha/E_c)^2 = 1.3 \times 10^{-10}$ nm^2, or a value of 1.3×10^{-24} cm^2.

The angular differential cross-section is obtained from the relationship between $d\Omega$ and $d\theta_c$ defined in Eqs. (4.6), $d\Omega = 2\pi\sin\theta_c\,d\theta_c$, and (4.20). Using some differential algebra we have

$$\frac{d\sigma(\theta_c)}{d\theta_c} = \frac{d\sigma(\theta_c)}{d\Omega}\frac{d\Omega}{d\theta_c} = 2\pi\left(\frac{\alpha}{2E_c}\right)^2\frac{\cos(\theta_c/2)}{\sin^3(\theta_c/2)} \tag{4.21}$$

Eqs. (4.20) and (4.21) are the Coulomb angular differential scattering cross-sections, otherwise known as the *Rutherford differential cross-sections*. From Eqs. (4.20) and (4.21) we see from the $\sin(\theta_c/2)$ term in the denominator that both $d\sigma(\theta_c)/d\theta_c$ and $d\sigma(\theta_c)/d\Omega$ increase as θ_c decreases. This indicates that the Coulomb scattering process favors small-angle scattering, or, in other words, the largest cross-sections are for scattering events of small angles.

For forward scattering with $\theta_c = 2$, $\sin^4(\theta_c/2) = 1 \times 10^7$, indicating a ratio of seven orders of magnitude between forward scattering at 2° and backscattering at 180°.

4.3 Energy-transfer differential scattering cross-section

In a fashion similar to the development of the angular differential scattering cross-section, we will derive an expression for the transferring of energy during a scattering event. Consider Fig. 4.6, where a flux of energetic incident particles traverses a thin target, of thickness dx and unit area, containing a total of N target atoms per unit volume. Each target nucleus presents an effective scattering area, σ, to this projectile, similar to the presentation in Fig. 4.2. The thin target in Fig. 4.6 contains a total of $N\,dx$ target nuclei per unit area. The product $\sigma N\,dx$ represents the total fraction of the target surface area which acts as an effective scattering center to the incident energetic particles.

From the above analysis of Fig. 4.6, we can define the probability of a projectile with energy E undergoing a scattering event or a collision with a target nucleus while traversing a thickness dx as

$$P(E) = N\sigma(E)\,dx \tag{4.22}$$

Eq. (4.22) defines the total collision cross-section, $\sigma(E)$, between an energetic particle of energy E and the target atoms. The total cross-section gives a measure of the probability for any type of collision to occur where energy transfers are possible, for energies up to and including the maximum value $T_M = 4M_1M_2E_0/(M_1 + M_2)^2$ (Eq. (3.27)).

In addition to the total cross-section, we also wish to consider the more restrictive types of interactions that can occur between particles with energy E and target nuclei. Consider the condition where we wish to know the probability that a projectile with energy E will transfer an amount of energy between T and $T + dT$ to a target atom. Such a

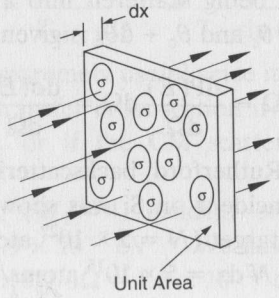

Fig. 4.6. Schematic view of a portion of a scattering foil, with each target atom presenting an effective scattering area σ.

probability function defines the differential energy-transfer cross-section $d\sigma(E)/dT$, and it is obtained by differentiating Eq. (4.22)

$$P(E, T)\,dT \equiv \frac{dP(E)}{dT}\,dT = N\frac{d\sigma(E)}{dT}\,dT\,dx = \frac{1}{\sigma(E)}\frac{d\sigma(E)}{dT}\,dT \tag{4.23}$$

where $P(E, T)$ is the probability that an ion with energy E will undergo a collision producing an energy transfer in the range T and $T + dT$ while traversing a distance dx, and is simply defined as the ratio of the differential cross-section to the total energy-transfer cross-section.

For the scattering processes described by Figs. 4.2 and 4.3, probability functions can be constructed which describe the probability of a collision producing a deflection θ_c in the incident projectile's trajectory or the probability of scattering the projectile into the angular range between θ_c and $\theta_c + d\theta_c$ while it travels a distance dx. These probability functions are given, respectively, by

$$P(\theta_c) = \sigma(\theta_c)N\,dx \tag{4.24a}$$

and

$$P(\theta_c, b)\,db \equiv \frac{dP(\theta_c)}{dp} = N\frac{d\sigma(\theta_c)}{dp}\,dp\,dx = \frac{1}{\sigma(\theta_c)}\frac{d\sigma(\theta_c)}{dp}\,dp \tag{4.24b}$$

where $\sigma(\theta_c)$ is the total angular scattering cross-section given in Eq. (4.3) and $d\sigma(\theta_c)$ is the differential angular scattering cross-section given in Eq. (4.4). An expression similar to Eq. (4.23) can also be constructed for the differential angular scattering cross-section as a function of the impact parameter.

Following an analogous route to the development of the differential energy cross-section given in Eq. (4.23), the probability function for a particle with energy E being scattered into a solid angle $d\Omega$ in the angular region between θ_c and $\theta_c + d\theta_c$ is given by

$$P(E, \Omega)\,d\Omega \equiv \frac{dP(E)}{d\Omega}\,d\Omega = \frac{d\sigma(E)}{d\Omega}N\,dx\,d\Omega \tag{4.25}$$

As an example, the Rutherford backscattering cross-section ($\sigma_c = 180°$) for 1 MeV ^{4}He incident on Si was shown to be 1.3×10^{-24} cm (Section 4.2). If the Si target ($N = 5 \times 10^{22}$ atoms/cm^3) is 10 nm thick ($dx = 10^{-6}$ cm), then $N\,dx = 5 \times 10^{16}$ atoms/cm^2. The probability, $P(E, \Omega)$, of this scattering event is 6.5×10^{-8}. For forward scattering at 2°, the corresponding probability is 0.65, indicating that nearly every

incident ion experiences a forward scattering event in traversing the film. As Eq. (4.25) shows, the probability of a scattering event occurring increases linearly with layer thickness.

The dependence on $d\Omega$ in Eq. (4.25) can be removed by applying Eq. (4.6), $d\Omega = 2\pi \sin\theta_c\,d\theta_c$, which allows us to write Eq. (4.25) as

$$P(E, \Omega)\,d\Omega = 2\pi N\,dx\frac{d\sigma(E)}{d\Omega} = 2\pi \sin\theta_c N\,dx\frac{d\sigma(E)}{d\Omega}\,d\theta_c \tag{4.26}$$

The relationship between energy transfer T and the scattering angle θ_c, or the solid angle Ω, can be found by setting the probability functions given by Eqs. (4.23) and (4.26) equal to each other:

$$P(E, T)\,dT = P(E, \Omega)\,d\Omega$$

which is equivalent to

$$\frac{d\sigma(E)}{dT}\,dT = 2\pi \sin\theta_c\,d\theta_c\frac{d\sigma(\theta_c)}{d\Omega}$$

or

$$\frac{d\sigma(E)}{dT} = 2\pi \sin\theta_c\left|\frac{d\theta_c}{dT}\right|\frac{d\sigma(\theta_c)}{d\Omega} \tag{4.27}$$

The transferred energy T is given in Eq. (3.26) as

$$T = T_M \sin^2(\theta_c/2) = \tfrac{1}{2}T_M(1 - \cos\theta_c)$$

and the differential angular cross-section for scattering into a solid angle $d\Omega$ is given by Eq. (4.7) as

$$\frac{d\sigma(\theta_c)}{d\Omega} = \frac{b}{\sin\theta_c}\left|\frac{db}{d\theta_c}\right|$$

which allows us to rewrite Eq. (4.27) in the form

$$\frac{d\sigma(E)}{dT} = \frac{4\pi}{T_M}\frac{d\sigma(\theta_c)}{d\Omega} = \frac{4\pi}{T_M}\frac{b}{\sin\theta_c}\left|\frac{db}{d\theta_c}\right| \tag{4.28}$$

This final expression is extremely useful since it allows us to determine the differential energy-transfer cross-section if the angular differential cross-section is known, or if the CM scattering angle and impact parameter are known.

For 1 MeV ^{4}He ions, ($M_1 = 4$) incident on Si ($M_2 = 28$), $T_M = 438$ keV and $4\pi/T_M = 2.9 \times 10^{-5}$ eV^{-1}. We have shown that for backscattering ($\theta_c = 180°$), $d\sigma(\theta_c)/d\Omega = 1.3 \times 10^{-24}$ cm^2. Thus, $d\sigma(E)/dT = 3.7 \times 10^{-29}$ cm^2/eV.

The total cross-section for a scattering process is determined by

setting the probability functions described by Eqs. (4.23) and (4.24b) equal to unity. This leads to

$$\sigma(E) = \int_{T_{\min}}^{T_M} \frac{d\sigma(E)}{dT}\, dT \tag{4.29a}$$

and

$$\sigma(\theta_c) = \int_{b_{\max}}^{0} \frac{d\sigma(\theta_c)}{db}\, db = \int_{b_{\max}}^{0} 2\pi b\, db \tag{4.29b}$$

where T_M is the maximum transferred energy, given by Eq. (3.27), $T_{\min}$ is a lower limit to the energy-transfer process, and $b_{\max}$ is the maximum impact parameter. The total cross-sections given by Eqs. (4.29a) and (4.29b) are equivalent, i.e., $\sigma(E) = \sigma(\theta_c)$. That is, integrating the energy-transfer differential cross-section over all energy transfers from $T_{\min}$ to T_M is the same as integrating over the range of impact parameters from $b_{\max}$ to zero. This equality between the total cross-sections provides a means for passing between the energy-transfer differential cross-section and the impact parameter.

4.4 Power law potentials and the impulse approximation

In this section we will examine the relationship between the potential $V(r)$ and the scattering angle θ_c for the collisions where $V(r)/E_c$ remains small throughout the entire collision process. This condition is realized for collisions where b is large, which in turn leads to small-angle scattering.

The scattering cross-section for central force scattering with large impact parameters can be calculated for small deflections from the impulse imparted to the particle as it passes the target nucleus. As the particle with charge Z_1e approaches the target nucleus, charge Z_2e, it will experience a repulsive force that will cause its trajectory to deviate from the incident straight line path (Fig. 4.7).

Let $\mathbf{p}_1$ and $\mathbf{p}_2$ be the initial and final momentum vectors of the particle. From Fig. 4.8(a) it is evident that the total change in momentum, $\Delta\mathbf{p} = \mathbf{p}_2 - \mathbf{p}_1$, is along the z' axis, which is the axis corresponding to the condition $r = r_{\min}$. In this calculation the magnitude of the momentum does not change. From the isosceles triangle formed by $\mathbf{P}_1$, $\mathbf{P}_2$, and $\Delta\mathbf{p}$ shown in Fig. 4.8(a) we have

$$\frac{\frac{1}{2}\Delta\mathbf{p}}{M\mathbf{v}} = \sin\frac{\theta_c}{2}$$

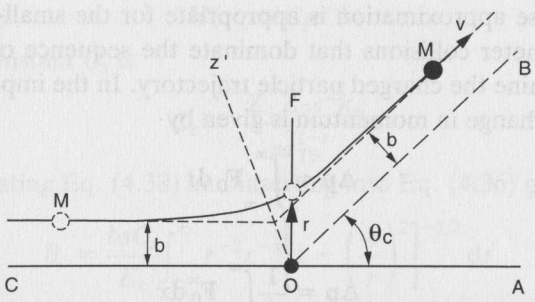

Fig. 4.7. The nucleus is assumed to be a point charge at the origin O. At any distance r, the particle experiences a repulsive force. The particle travels along a path that is initially parallel to line OA a distance b from it and finally parallel to line OB, which makes an angle θ_c with OA.

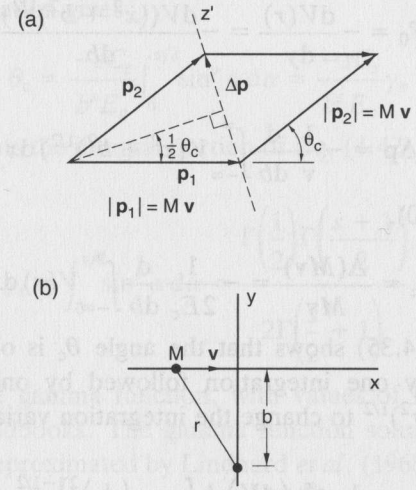

Fig. 4.8. (a) Momentum diagram for impulse scattering (see Fig. 4.7). Note that $|\mathbf{p}_1| = |\mathbf{p}_2|$, i.e., for elastic scattering the energy and speed of the projectile are the same before and after the collision. (b) Change-of-variable diagram for momentum (impulse) approximation.

or, in the limit of $\theta_c \ll 1$,

$$\frac{\Delta\mathbf{p}}{M\mathbf{v}} = \frac{\Delta(M\mathbf{v})}{M\mathbf{v}} \cong \theta_c \tag{4.30}$$

Eq. (4.30) indicates that, at small deflections, θ_c can be thought of as being due to a small impulse, $\Delta\mathbf{p} = \Delta(M\mathbf{v})$, approximately perpendicular to the original direction of motion. This small-angle calculation is commonly called the *impulse* or *momentum approximation*.

The impulse approximation is appropriate for the small-angle large-impact-parameter collisions that dominate the sequence of scatterings which determine the charged particle trajectory. In the impulse approximation the change in momentum is given by

$$\Delta \mathbf{p} = \int_{-\infty}^{\infty} \mathbf{F}_0 \, \mathrm{d}t \tag{4.31}$$

or

$$\Delta \mathbf{p} = \frac{1}{\mathbf{v}} \int_{-\infty}^{\infty} \mathbf{F}_0 \, \mathrm{d}x \tag{4.32}$$

where $\mathbf{F}_0$ is the component of the force acting on the ion perpendicular to its incident direction. By using the geometry of Fig. 4.8(b), the force may be written with $r = (x^2 + b^2)^{1/2}$ as

$$\mathbf{F}_0 = -\frac{\mathrm{d}V(r)}{\mathrm{d}y} = -\frac{\mathrm{d}V((x^2 + b^2)^{1/2})}{\mathrm{d}b} \tag{4.33}$$

Then

$$\Delta \mathbf{p} = -\frac{1}{\mathbf{v}} \frac{\mathrm{d}}{\mathrm{d}b} \int_{-\infty}^{\infty} V(x^2 + b^2)^{1/2}) \, \mathrm{d}x \tag{4.34}$$

or, using Eq. (4.30),

$$\theta_c = \frac{\Delta(M\mathbf{v})}{M\mathbf{v}} = -\frac{1}{2E_c} \frac{\mathrm{d}}{\mathrm{d}b} \int_{-\infty}^{\infty} V(r) \, \mathrm{d}x \tag{4.35}$$

for $\theta_c \ll 1$. Eq. (4.35) shows that the angle θ_c is obtained from the potential $V(r)$ by one integration followed by one differentiation. Using $r = (x^2 + y^2)^{1/2}$ to change the integration variable in Eq. (4.35) yields

$$\theta_c = \frac{1}{E_c} \int_{-\infty}^{\infty} \left(\frac{\mathrm{d}V}{\mathrm{d}r}\right) \frac{b}{r} \left[1 - \left(\frac{b}{r}\right)^2\right]^{-1/2} \mathrm{d}r \tag{4.36}$$

Eq. (4.36) is often referred to as the classical impulse approximation to the scattering integral.

Consider now a screened Coulomb potential of the type $V(r) \propto r^{-1}$, where the screening function can be approximated by the power form given in Eq. (2.37)

$$\chi(r/a_{TF}) = \frac{k_s}{s} \left(\frac{a_{TF}}{r}\right)^{s-1} \tag{4.37}$$

where $s = 1, 2, \ldots$, k_s is a numerical constant, and a_{TF} is the screening radius given by Eq. (2.43). The screened Coulomb potential can be written as

$$V(r) = C_s r^{-s} \tag{4.38}$$

where the constant C_s is

$$C_s = \frac{Z_1 Z_2 e^2 k_s}{s a_{TF}^{1-s}} \tag{4.39}$$

Differentiating Eq. (4.38) and inserting into Eq. (4.36) gives

$$\theta_c = \frac{bsC_s}{E_c} \int_{-\infty}^{\infty} r^{-2} r^{-s} \left[1 - \left(\frac{b}{r}\right)^2\right]^{-1/2} \mathrm{d}r \tag{4.40}$$

To solve Eq. (4.40) will require the following change of variable:

$$r = \frac{b}{\sin \alpha} \tag{4.41}$$

where b is the impact parameter and α is a dummy variable. Carrying out the transformation gives

$$\theta_c = \frac{-sC_s}{b^s E_c} \int_0^{\pi/2} \sin^s \alpha \, \mathrm{d}\alpha = \frac{-sC_s}{b^s E_c} \gamma_s \tag{4.42}$$

where γ_s represents the integral portion of Eq. (4.42) and has the exact solution

$$\gamma_s = \int_0^{\pi/2} \sin^s \alpha \, \mathrm{d}\alpha = \frac{\Gamma\left(\frac{1}{2}\right)\Gamma\left(\frac{s+1}{2}\right)}{2\Gamma\left(\frac{s}{2} + 1\right)} \tag{4.43}$$

where $\Gamma(x)$ is the gamma function, with values of $\Gamma(x)$ tabulated in mathematical handbooks. The gamma function solution given in Eq. (4.43) has been approximated by Lindhard *et al.* (1968)

$$\gamma_s \cong \frac{1}{s} \left(\frac{3s - 1}{2}\right)^{1/2} \tag{4.44}$$

Combining Eqs. (4.39) and (4.42) allows us to write the scattering angle equation in the compact form

$$\theta_c = \frac{\gamma_s k_s}{\varepsilon} \left(\frac{a_{TF}}{b}\right)^s \tag{4.45}$$

where ε is the reduced energy, initially defined in Eq. (3.55):

$$\varepsilon = \frac{a_{TF} E_c}{Z_1 Z_2 e^2}$$

The angular differential cross-section can now be derived for the power law potential using the differential cross-section $\mathrm{d}\sigma(\theta_c)$, Eq.

(4.5), and Eq. (4.45). Rewriting Eq. (4.45) in terms of the impact parameter b

$$b = a_{TF}\left(\frac{\gamma_s k_s}{\varepsilon\theta_c}\right)^{1/s} \tag{4.46}$$

and differentiating b with respect to θ_c

$$\left|\frac{db}{d\theta}\right| = \frac{a_{TF}}{s}\left(\frac{\gamma_s k_s}{\varepsilon}\right)^{1/s}\frac{1}{\theta_c^{1/s+1}} \tag{4.47}$$

The angular differential cross-section is

$$d\sigma(\theta_c) = 2\pi b\left|\frac{db}{d\theta_c}\right| d\theta_c = C_0\left(\frac{a_{TF}^2}{\varepsilon^{2/s}\theta_c^{1+2/s}}\right) d\theta_c \tag{4.48}$$

where C_0 is a constant given by

$$C_0 = \frac{2\pi}{s}(\gamma_s k_s)^{2/s} \tag{4.49}$$

4.5 Power law energy-transfer cross-section

The power law potential energy-transfer differential cross-section can be obtained using Eq. (4.48) and the CM energy-transfer function, Eq. (3.26),

$$T = T_M \sin^2\frac{\theta_c}{2} \tag{4.50}$$

In the small-angle limit,

$$\left(\frac{T}{T_M}\right)^{1/2} = \sin\frac{\theta_c}{2} \cong \frac{\theta_c}{2} \quad \text{for } \theta_c \ll 1 \tag{4.51}$$

Solving for θ_c

$$\theta_c = 2\left(\frac{T}{T_M}\right)^{1/2} \tag{4.52}$$

taking the differential with respect to T

$$d\theta_c = \frac{dT}{(T/T_M)^{1/2}} \tag{4.53}$$

and substituting into Eq. (4.48)

$$d\sigma(E) = C_0\frac{a_{TF}^2}{\varepsilon^{2/s}}\frac{T_M^{1/s}}{T^{1+1/s}}dT \tag{4.54}$$

Rewriting Eq. (4.54) in terms of the laboratory energy E_0 and noting that (Eq. (3.27))

$$T_M = \frac{4M_1M_2}{(M_1+M_2)^2}E_0$$

and from Eq. (3.35)

$$\varepsilon = \left(\frac{a_{TF}}{Z_1Z_2e^2}\right)\left(\frac{M_2E_0}{M_1+M_2}\right)$$

we obtain

$$d\sigma(E) = \frac{C_m}{E^m T^{1+m}}dT \tag{4.55}$$

where $m = 1/s$. The constant C_m is given by

$$C_m = \frac{\pi}{2}\lambda_m a_{TF}^2\left(\frac{2Z_1Z_2e^2}{a_{TF}}\right)^{2m}\left(\frac{M_1}{M_2}\right)^m \tag{4.56}$$

where λ_m is a fitting variable given by

$$\lambda_m = 2m\left(\frac{k_s\gamma_s}{2}\right)^{2m} \tag{4.57}$$

If $\chi(r)$ is taken as the Thomas–Fermi screening function, good fits to the constant k_s over various distances corresponding to the range of ions yield (Winterbon *et al.*, 1970).

$$\lambda_{1/3} = 1.309; \quad \lambda_{1/2} = 0.327; \quad \lambda_1 = 0.5 \tag{4.58}$$

Winterbon *et al.* (1970) recommend the following values of m for various regions of ε:

$m = 1/3$ for $\varepsilon \leqslant 0.2$

$m = 1/2$ for $0.08 \leqslant \varepsilon \leqslant 2$

$m = 1$ (Rutherford scattering) for $\varepsilon \geqslant 10$

The validity of Eq. (4.54) can be determined by considering Rutherford scattering where the potential is unscreened Coulomb. The power parameter for this potential is $s = m = 1$. In this case the screening function, Eq. (4.37), is 1 and therefore $k_1 = 1$. From Eq. (4.44), $\gamma_1 = 1$, and C_0 is simply equal to 2π. For $s = 1$, Eq. (4.56) reduces to

$$C_1 = \frac{\pi}{4}(2Z_1Z_2e^2)^2\frac{M_1}{M_2} \tag{4.59}$$

For the pure Coulomb condition, the power law equation, Eq. (4.55), reduces to

$$d\sigma(E) = \frac{\pi}{4}(2Z_1Z_2e^2)^2\frac{M_1}{M_2}\frac{dT}{E_0T^2} \tag{4.60}$$

We now compare this result with the differential energy-transfer cross-section obtained using the Rutherford cross-section given by Eq. (4.20),

$$d\sigma(\theta_c) = \left(\frac{\alpha}{4E_c}\right)^2 \frac{d\Omega}{\sin^4(\theta_c/2)}$$

The transformation from $d\sigma(\theta_c)/d\Omega$ to $d\sigma(\theta_c)/dT$ is made with the help of Eq. (4.28)

$$\frac{d\sigma(E)}{dT} = \frac{4\pi}{T_M}\frac{d\sigma(\theta_c)}{d\Omega}$$

which allows us to write the differential of the energy-transfer function with respect to the scattering angle for the Coulomb potential as

$$d\sigma(E) = \left(\frac{\alpha}{4E_c}\right)^2 \frac{4\pi T_M\, dT}{T_M^2 \sin^4(\theta_c/2)} = \frac{\pi}{4}\left(\frac{\alpha}{E_c}\right)^2 \frac{T_M}{T^2} dT$$

Substituting for E_c, T_M, and α gives

$$E_c = \frac{M_2 E_0}{M_1 + M_2}$$

$$T_M = \frac{4M_1M_2}{(M_1 + M_2)^2} E_0$$

$$\alpha = Z_1 Z_2 e^2$$

which leads to

$$d\sigma(E) = \frac{\pi}{4}(2Z_1Z_2e^2)^2 \frac{M_1}{M_2 E_0 T^2} dT$$

A comparison of this result with the power law derived equation, Eq. (4.60), shows them to be identical.

4.6 Reduced cross-section

As the previous sections have shown, the power law potential can greatly simplify the calculation of the energy-transfer differential cross-section. However, the differential cross-section is still a function of six major parameters: $d\sigma = f(Z_1, Z_2, E, \theta_c, M_1, M_2)$. To simplify differential cross-section calculations even further, J. Lindhard, V. Nielsen, and M. Scharff introduced a universal one-parameter differential scattering cross-section equation in reduced notation:

$$d\sigma = \frac{-\pi a_{TF}^2}{2} \frac{f(t^{1/2})}{t^{3/2}} dt \qquad (4.61)$$

Table 4.1. *Thomas–Fermi scattering function* $f(t^{1/2})$

$t^{1/2}$	$f(t^{1/2})$
0.002	0.162
0.004	0.209
0.01	0.280
0.02	0.334
0.04	0.383
0.10	0.431
0.15	0.435
0.20	0.428
0.40	0.385
1	0.275
2	0.184
4	0.107
10	0.050
20	0.025
40	0.0125

After Lindhard *et al.* (1968).

where t is a dimensionless collision parameter defined by

$$t \equiv \varepsilon^2 \frac{T}{T_M} = \varepsilon^2 \sin^2\left(\frac{\theta_c}{2}\right) \qquad (4.62)$$

where T is the transferred energy, T_M is the maximum transferred energy, and ε is the dimensionless energy unit defined in Eq. (3.55) as

$$\varepsilon \equiv \frac{a_{TF}}{d_c} = \frac{a_{TF} E_c}{Z_1 Z_2 e^2}$$

In the above expression, d_c is the unscreened (i.e., Coulomb) collision diameter or distance of closest approach for a head-on collision (i.e., $b = 0$), and a_{TF} is the screening distance.

Lindhard *et al.* (1968) considered $f(t^{1/2})$ to be a simple scaling function and the variable t to be a measure of the depth of penetration into the atom during a collision, with large values of t representing small distances of approach. Tabulated data for $f(t^{1/2})$ for the Thomas–Fermi atom are presented in Table 4.1. Fig. 4.9 shows a plot of the tabulated data together with an analytical approximation (Winterbon *et al.*, 1970)

$$f(t^{1/2}) = \lambda' t^{1/6}[1 + (2\lambda' t^{2/3})^{2/3}]^{-3/2} \qquad (4.63)$$

where

$$\lambda' = 1.309$$

Also plotted in Fig. 4.9 are the various forms of $f(t^{1/2})$ for power law scattering. At small values of t, the function $f(t^{1/2})$ asymptotically approaches $f(t^{1/2}) = \lambda' t^{1/6}$, which is a special case of the more general power law approximation

$$f(t^{1/2}) = \lambda_m t^{1/2-m} \tag{4.64}$$

where the values for λ_m are listed in Eq. (4.58) and $\lambda' = \lambda_{1/3}$. Eq. (4.64) approximately describes scattering from a potential of the form $V(r) \propto r^{-s} = r^{-1/m}$. At low energies the collisions become less penetrating (small t), and the scattering by screened Coulomb potentials is determined by regions with large values of s. In this situation the interaction during collisions involves the outer part of the atom and increases with increasing t. For high-energy collisions, where $s < 2$, screening effects are minimal since interactions primarily involve the inner parts of the atom, and $f(t^{1/2})$ decreases with increasing t.

On examining Fig. 4.9, we see that the potential of the form $V(r) \propto r^{-3}$ (i.e., $m = 1/3$) is an excellent approximation to the

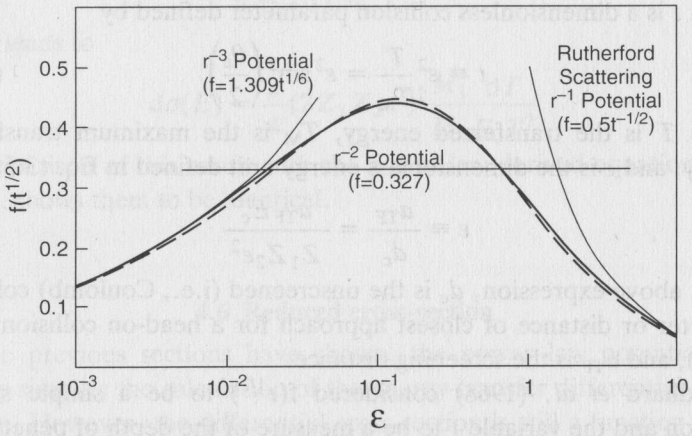

Fig. 4.9. Reduced differential cross-section calculated from Thomas–Fermi potential. Ordinate is $f(t^{1/2}) = 2t^{2/3}\, d\sigma/dt(\pi a^2)^{-1}$; abscissa is $\varepsilon = t^{1/2}/\sin(\theta/2)$. Thick solid line ranging over $\varepsilon = 10^{-3}$–10: Eq. (4.61). Dashed line: Eq. (4.63). Thin solid lines are calculated using the power law cross-section formula, Eq. (4.64). For large values of $t^{1/2}$ (i.e., large ε), the curve approaches Rutherford scattering (i.e., an r^{-1} potential), while at small values of $t^{1/2}$ (i.e., small ε), the curve approaches an r^{-3} potential. The horizontal line represents $f(t^{1/2})$ for an r^{-2} potential. (After Winterbon *et al.*, 1970.)

Table 4.2. *Fitting parameters for the scattering function* $f(t^{1/2})$

Screening function	γ	m	q	$t^{1/2}$ range
Thomas–Fermi	1.309	0.333	0.667	10^{-3}–10
Bohr, Eq. (2.38)	2.37	0.103	0.570	10^{-3}–10
Lenz–Jensen, Eq. (2.39)	2.92	0.191	0.512	10^{-3}–10
Lindhard, Eq. (2.33)	0.625	0.333	1.24	10^{-3}–10
Lindhard, Eq. (2.34)	0.879	0.333	1.24	10^{-3}–10
Moliere, Eq. (2.36)	3.07	0.216	0.530	10^{-3}–10
KO[a]	2.54	0.25	0.475	10^{-5}–10
ZBL, Eq. (2.52)	5.01	0.203	0.413	10^{-6}–10^{4}
Kr-C[b]	3.35	0.233	0.445	10^{-6}–10^{4}

After Winterbon (1972).
[a]Kalbitzer and Oetzmann (1980).
[b]Littmark and Ziegler (1981); Wilson *et al.* (1977).

Thomas–Fermi function $f(t^{1/2})$ at small values of t. Fig. 4.9 also shows that when $s = 2$ ($m = 1/2$), $f(t^{1/2})$ = constant = 0.327, which is a reasonable overall approximation, and for $s = 1$ the unscreened Coulomb potential (Rutherford scattering) is approximate for $t \gg 1$.

The Thomas–Fermi function $f(t^{1/2})$ described by Eq. (4.63) can be generalized to provide a one-parameter universal differential scattering cross-section equation for other interatomic potentials. The general form of Eq. (4.63) is

$$f(t^{1/2}) = \lambda t^{1/2-m}[1 + (2\lambda t^{1-m})^q]^{-1/q} \tag{4.65}$$

where λ, m, and q are fitting variables, with $\lambda = 1.309$, $m = 1/3$ and $q = 2/3$ for the Thomas–Fermi version of $f(t^{1/2})$ given in Eq. (4.63). Additional values for λ, m, and q for other forms of the screening function are presented in Table 4.2.

4.7 Hard-sphere potential

In some problems in ion–solid interactions, a great deal of physical insight can be obtained by assuming that the projectile and target atoms interact like colliding billiard balls (elastic hard spheres). The interatomic potential which represents this condition is the *hard-sphere* potential given in Eq. (2.6). The hard-sphere approximation is most applicable for near head-on collisions, with the impact parameter b approaching zero and the scattering angle θ_c approaching π (see Fig. 3.7(b)).

A hard-sphere collision in the center of mass (CM) between two particles with masses M_1 and M_2 and radii R_1 and R_2 is displayed in Fig. 4.10. For a hard-sphere collision, the distance of closest approach is given by

$$r_{\min} = r_1 + r_2 \tag{4.66}$$

where $r_1 = R_1$ and $r_2 = R_2$. Comparing Figs. 4.10 and 3.7(b), we see that r_1 and r_2 can be defined by Eq. (3.42), where r is replaced by $r_{\min}$

$$r_1 = \frac{M_2}{M_1 + M_2} r_{\min} \tag{4.67a}$$

and

$$r_2 = \frac{M_1}{M_1 + M_2} r_{\min} \tag{4.67b}$$

From Figs. 2.2(a) and 4.10, we see that the interaction potential energy will only apply at contact between the hard spheres. The hard-sphere potential energy is simply equal to the CM kinetic energy, Eq. (3.16b),

$$V(r_{\min}) = \frac{M_2}{M_1 + M_2} E_0 \tag{4.68}$$

The relationship between the impact parameter b and $r_{\min}$ is obtained from Fig. 4.10:

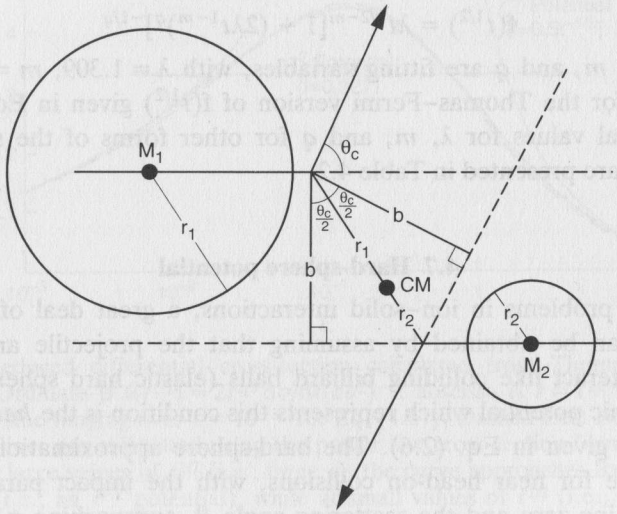

Fig. 4.10. The hard-sphere scattering geometry.

$$b = r_{\min} \cos\left(\frac{\theta_c}{2}\right) \tag{4.69}$$

The angular differential cross-section is obtained by differentiating Eq. (4.69) and using Eq. (4.5):

$$d\sigma(\theta_c) = \pi r_{\min}^2 \sin\frac{\theta_c}{2} \cos\frac{\theta_c}{2} d\theta \tag{4.70}$$

The energy-transfer differential cross-section is obtained by differentiating Eq. (4.69) and using Eq. (4.28):

$$\frac{d\sigma(E)}{dT} = \frac{\pi r_{\min}^2}{T_M} \tag{4.71}$$

The total collisional cross-section for a particle with energy E transferring energy T can be approximated following Eq. (4.3):

$$\sigma(E) \cong \pi r_{\min}^2 \tag{4.72}$$

Combining Eqs. (4.71) and (4.72) with Eq. (4.23), we can easily calculate the hard-sphere probability of an energetic particle with energy E producing a recoil in the energy range between T and $T + dT$:

$$P(E, T)\, dT = \frac{1}{\sigma(E)} \frac{d\sigma(E)}{dT} dT \cong \frac{dT}{T_M} \tag{4.73}$$

The major advantage of Eqs. (4.71)–(4.73) is their lack of dependence on E, which simplifies the integration needed in calculating energy-loss and radiation-damage values in Chapters 5 and 7.

References

Kalbitzer, S. and H. Oetzmann (1980) Ranges and Range Theories, *Radiation Effects* **47**, 57.

Lindhard, J., V. Nielsen, and M. Scharff (1968) Approximation Method in Classical Scattering by Screened Coulomb Fields (notes on Atomic Collisions I), *Mat. Fys. Medd. Dan Vid. Selsk.* **36**, no. 10.

Littmark, V. and J. F. Ziegler (1981) Ranges of Energetic Ions in Matter, *Phys. Rev.* **A23**, 64.

Wilson, W. D., L. G. Haggmark, and J. P. Biersack (1977) Calculations of Nuclear Stopping, Ranges, and Straggling in the Low-Energy Region, *Phys. Rev.* **B15**, 2458.

Winterbon, K. B. (1972) Heavy-Ion Range Profiles and Associated Damage Distributions, *Radiation Effects* **13**, 215.

Winterbon, K. B., P. Sigmund, and J. B. Sanders (1970) Spacial Distribution of Energy Deposited by Atomic Particles in Elastic Collisions, *Mat. Fys. Medd. Dan Vid. Selsk.* **37**, no. 14.

Suggested reading

Classical Mechanics, H. Goldstein (Addison-Wesley Publishing Co., Reading, Mass., 1959).
Collision Theory of Displacement Damage, Ion Ranges and Sputtering, P. Sigmund, *Rev. Roumaine Phys.* **17**, pp. 823, 969 & 1079 (1972).
Defects and Radiation Damage in Metals, M. W. Thompson (Cambridge University Press, 1969).
Elementary Modern Physics, R. T. Weidner and R. L. Sells (Allyn & Bacon Inc., Boston, 1980), 3rd edn.
Fundamental Aspects of Nuclear Reactor Fuel Elements, D. R. Olander (National Technical Information Service, Springfield, Virginia, 1976), chap. 17.
Fundamentals of Surface and Thin Film Analyses, L. C. Feldman and J. W. Mayer (North-Holland Science Publishing, New York, 1986).
Interatomic Potentials, I. M. Torrens (Academic Press, New York, 1972).
Introduction to Atomic and Molecular Collisions, R. E. Johnson (Plenum Press, New York, 1982).
Mechanics, K. R. Symon (Addison-Wesley Publishing Co., Reading, Mass., 1953).
Newtonian Mechanics, A. P. French (W. W. Norton & Co., New York, 1971).
The Stopping and Range of Ions in Solids, J. F. Ziegler, J. P. Biersack, and U. Littmark (Pergamon Press Inc., New York, 1985).

Problems

4.1 Using Eq. (4.20), calculate the differential scattering cross-section per solid angle for 100 keV Ar ions incident on Ni for laboratory scattering angles of 10°, 15°, 45°.

4.2 Using Eq. (4.25), calculate the probability $P(E, \Omega)$ for 100 keV Ar ions incident on Ni for laboratory scattering angles of 10° and 45° for Ni thicknesses of 10 and 100 nm.

4.3 Show that Eq. (4.61) can be written in the form

$$d\sigma = \frac{\pi a^2}{2} \frac{T_M^{1/2}}{\varepsilon} \frac{f(t^{1/2})}{T^{3/2}} dT$$

4.4 For $M_1 < M_2$ (He on Si), $M_1 = M_2$ (Si on Si), and $M_1 > M_2$ (Xe on Si), calculate values of the dimensionless collision parameter t, θ_c, and the laboratory scattering angle, θ, for values of $T/T_M = 0.25$, 0.5, and 0.75 (Eq. (4.62)). Assume $E_0 = 100$ keV in all cases.

4.5 Using values from problem 4.4 and Table 4.1, calculate $d\sigma/dT$.

4.6 Solve the power law cross-section, Eq. (4.55), for the hard-sphere power law parameter $m = 0$ and compare with Eq. (4.71) to find C_0.

4.7 From the Coulomb cross-section described in Eq. (4.60), derive a general expression for the total cross-section using Eq. (4.29).

4.8 For 1 MeV ^{4}He ions on Si, what is $\sigma(E)$ for $T_{min} = 15$ eV (see problem 4.7)?